Cortical Folding of the Primate Brain: An Interdisciplinary Examination of the Genetic Architecture, Modularity, and Evolvability of a Significant Neurological Trait in Pedigreed Baboons (Genus *Papio*)

Elizabeth G. Atkinson,*,[1] Jeffrey Rogers,[†] Michael C. Mahaney,[‡,§] Laura A. Cox,[§] and James M. Cheverud*,**

*Department of Anatomy and Neurobiology, Washington University in St. Louis School of Medicine, St. Louis, Missouri 63110, [†]Human Genome Sequencing Center and Department of Molecular and Human Genetics, Baylor College of Medicine, Houston, Texas 77030, [‡]South Texas Diabetes and Obesity Institute, University of Texas Health Science Center at San Antonio and Regional Academic Health Center, Harlingen, Texas 78550, [§]Department of Genetics and Southwest National Primate Research Center, Texas Biomedical Research Institute, San Antonio, Texas 78245, and **Department of Biology, Loyola University, Chicago, Illinois 60660

ABSTRACT Folding of the primate brain cortex allows for improved neural processing power by increasing cortical surface area for the allocation of neurons. The arrangement of folds (sulci) and ridges (gyri) across the cerebral cortex is thought to reflect the underlying neural network. Gyrification, an adaptive trait with a unique evolutionary history, is affected by genetic factors different from those affecting brain volume. Using a large pedigreed population of ~1000 *Papio* baboons, we address critical questions about the genetic architecture of primate brain folding, the interplay between genetics, brain anatomy, development, patterns of cortical–cortical connectivity, and gyrification's potential for future evolution. Through Mantel testing and cluster analyses, we find that the baboon cortex is quite evolvable, with high integration between the genotype and phenotype. We further find significantly similar partitioning of variation between cortical development, anatomy, and connectivity, supporting the predictions of tension-based models for sulcal development. We identify a significant, moderate degree of genetic control over variation in sulcal length, with gyrus-shape features being more susceptible to environmental effects. Finally, through QTL mapping, we identify novel chromosomal regions affecting variation in brain folding. The most significant QTL contain compelling candidate genes, including gene clusters associated with Williams and Down syndromes. The QTL distribution suggests a complex genetic architecture for gyrification with both polygeny and pleiotropy. Our results provide a solid preliminary characterization of the genetic basis of primate brain folding, a unique and biomedically relevant phenotype with significant implications in primate brain evolution.

KEYWORDS gyrification; QTL; cerebral cortex; heritability; primate brain; evolution; modularity; *Papio hamadryas*

THE extent of folding of the cerebral cortex, known as "cortical gyrification," has dramatically increased during primate evolution, in parallel with increasing brain volumes. The cortex of Old World monkeys is significantly more folded (gyrified) than that of New World monkeys (Zilles *et al.* 1989; Martin 1990), and the great apes have the highest degree of gyrification in nonhuman primates (Preuss *et al.* 2004). Humans are outliers even within the primate clade, with our brain being almost 30% more folded than that of chimps (Rogers *et al.* 2010). Powerful physical constraints on the upper limit of human neonatal brain volume drive selection toward the most compact brain possible (Rosenberg and Trevathan 2002), while humankind's ecological niche demands high cognitive potential. Since the cell bodies of neurons–the functional units of information processing in the brain–are located in the outermost layer of the laminar brain system, folding

doi: 10.1534/genetics.114.173443
Manuscript received December 7, 2014; accepted for publication April 8, 2015; published Early Online April 14, 2015.
Supporting information is available online at www.genetics.org/lookup/suppl/doi:10.1534/genetics.114.173443/-/DC1.
[1]Corresponding author: Department of Ecology and Evolution—Office #631, Life Science Bldg., Stony Brook University, Stony Brook, NY 11794.
E-mail: elizabeth.atkinson@stonybrook.edu.

the cerebral cortex is an effective method of increasing surface area in which to allocate neurons with minimal overall brain volume expansion.

Selection for a larger brain volume does not automatically create one that is more folded. In fact, in baboons, genetic changes associated with increased brain size have been shown to result in a cortex with fewer folds (Rogers *et al.* 2010). Human congenital abnormalities also demonstrate the separation of these two phenotypes: conditions of abnormal brain volumes typically present with normal gyrification and vice versa (Stevenson 2006). These findings suggest that gyrification has a separate genetic basis from brain size, so the trend of increased folding in the primate lineage involves selective forces that have been working separately but in tandem with those increasing gross brain volume. While there has been extensive work examining changes in brain size among primates, cortical gyrification has a unique evolutionary history that has not yet been broadly explored.

Previous studies using magnetic resonance (MR) imaging provide preliminary evidence for a heritable genetic component to cortical variation in the baboon population studied here, generally estimating the heritability of cortical morphological features as between 20 and 40% (Mahaney *et al.* 1993; Rogers *et al.* 2007; Kochunov *et al.* 2010). As only ~150 MR scans were previously available, however, precise genetic mapping was impossible. By expanding the sample to glean information from ~1000 skull computed tomography (CT) scans collected in this pedigreed population, we were able to thoroughly assess variation and conduct QTL mapping to isolate defined chromosome regions affecting cortical gyrification phenotypes. QTL techniques are useful in that they provide an unbiased way to discover novel genomic regions associated with traits of interest in addition to implicating known genes in performing unanticipated novel functions. Additionally, conditions of dominance and epistatic interactions can be assessed and the power and strength of a genetic association to the phenotype quantified. The pedigree of the baboon population with which we are working includes six generations, resulting in a genomic linkage map (Rogers *et al.* 2000; Cox *et al.* 2006) that is quite well saturated with molecular markers thanks to the many resultant recombination events. This allowed us to isolate relatively narrow regions of interest containing small numbers of candidate genes. The advantage of pedigree-based linkage analyses lies in the fact that variants can be examined directly using identity-by-descent information rather than relying on variant state as a proxy. Furthermore, the effect size attributable to the implicated chromosomal regions can be reasonably estimated and situations of polygeny and/or pleiotropy detected.

Gyrification is extremely interesting from an evolutionary perspective for its neurobiological implications. Not only is increased gyrification useful for fitting more neurons within the skull, but patterns of sulci and gyri have direct implications with regard to the neural network (Ventura-Antunes *et al.* 2013). As would be expected from a trait that is at least partially controlled by genetic variation, sulci are not randomly distributed across the cortex; consistent folds appear within species and the degree and pattern of cortical folding shows phylogenetic trends in primates (Zilles *et al.* 1989, 2013; Krubitzer 2009; Chen *et al.* 2013). There are a number of hypotheses explaining the mechanisms behind the development of cortical gyrification and why sulci appear where they do, many involving mechanical tension on axonal tracts, the neuronal connections that allow communication between brain regions. The original tension-based hypothesis proposed by Van Essen (1997) posits that these white-matter tracts place tension on the laminar cortical surface layers, pulling regions together more strongly if more axons pass between them. The presence of mechanical tension on connectivity tracts between brain cells has been demonstrated empirically both *in vitro* (Heidemann and Buxbaum 1990, 1994; Herculano-Houzel *et al.* 2010) and *in vivo* (Xu *et al.* 2009, 2010) in addition to fitting with computational models of gyrification (Hilgetag and Barbas 2006; Mota and Herculano-Houzel 2012). Therefore, extending the hypothesis to an evolutionary viewpoint, if there is pressure for increased folding, the path of least physical resistance would be for sulci to form that separate the regions of lowest mechanical tension, *i.e.*, those with low connectivity. Functional connectivity would therefore parallel anatomical propinquity (Van Essen 1997; Hilgetag and Barbas 2006; Toro *et al.* 2008; Herculano-Houzel *et al.* 2010; Mota and Herculano-Houzel 2012; Zilles *et al.* 2013), meaning that the gyrification pattern is a direct external proxy for the underlying neural network.

Ultimately, the final adult gyrification pattern depends on the genetic and developmental processes underlying these traits. Modularity is ubiquitous in biological systems, including brain networks (Zhou *et al.* 2006; Chen *et al.* 2008; Meunier *et al.* 2009, 2010). It has been proposed that modularity would lead to the minimum possible distances between interacting regions of the cortex as an adaptive scheme for efficient neural processing (Sporns *et al.* 2004; Meunier *et al.* 2010). Indeed, it has been shown that anatomical proximity is associated with a higher number of connecting axons (Markov *et al.* 2011, 2014). Elucidating the exact structure of modularity and the location of module borders over the cortex, as is done in this study, exposes both the historical pattern of selection on brain features and the potential constraints imposed on future evolutionary alteration of the cerebrum. For example, if traits are within the same genetic module—*i.e.*, they are controlled by the same gene or set of genes—it is difficult to modify them independently of one another because a mutation will have a corresponding effect on both traits. Traits that have a history of close interaction should group into the same cluster while those experiencing different selective pressures should theoretically fall into separate modules. Thus, defining and comparing the borders of cortical-folding modules across biological domains (genetic, anatomical, developmental, connectivity) has significant implications for the ease of future adaptive alteration of the cortex by elucidating potential constraints on the full breadth of phenotypic space that can be explored.

If traits function together during life or develop together, the principle of morphological integration predicts that they will also be inherited together due to the pleiotropic effects of common genes (Cheverud 1996; Wagner 1996; Barton 2006; Wagner *et al.* 2007; Klingenberg 2008). Similarly, if sulcal formation is indeed guided by axonal tension related to the number of tracts uniting regions during development, then one should suspect that a similar pattern of variation will occur in sulcal anatomy, developmental programs, and the pattern of intrahemispheric connectivity. Here, we statistically test these predictions of a tension-based model for sulcal development and assess the degree of morphological integration of the baboon's cortex across the biological domains of phenotype, genotype, anatomy, connectivity, and development. Specifically, a similar partitioning of variation between anatomy (location of individual sulci in the context of a hemisphere), connectivity (number of axonal tracts connecting specific regions), and development (embryonic day of appearance of the sulcus) would support an interrelationship predicted by such a model.

This study sheds light on the genetic architecture underlying cortical gyrification in baboons. Specifically, we examine the structure of modularity over gyrification across biological domains and the interplay between domains (relevant to the ease of altering the shape of gyrification in response to particular evolutionary selective pressures), estimate the quantitative genetic effect on variation in cortical folding, and identify novel DNA regions associated with gyrification in this primate species. Such characterization provides a solid framework for future studies that seek to delve into the sequence evolution and function of candidate genes affecting brain topology and provides a more thorough understanding of the genetics underlying the evolution of brain folding and its consequences for function. Our results have medical implications for the many congenital disorders associated with abnormal cortical gyrification.

Materials and Methods

Study population and pedigree details

The study population consists of olive baboons, *Papio hamadryas anubis*, and yellow baboons, *P. h. cynocephalus*, and their hybrids living in the Southwest National Primate Research Center (SNPRC) in San Antonio, Texas. Although there has been considerable debate over the classification of olive and yellow baboons as either separate species or subspecies of *P. hamadryas*, we are here considering them as subspecies, as they are found to freely and successfully interbreed in the wild, in captivity, and in our study population (Alberts and Altmann 2001; Groves 2001; Jolly 2001; Charpentier *et al.* 2012). There are currently ~1600 animals living at the facility that are part of a managed breeding endeavor that has produced a full six-generation pedigree. The colony is divided into group cages of 10–30 adult females and their young offspring with one male, which results in the least amount of aggression between animals and assists in determining paternity of offspring. The population is maintained with an adult female:male ratio of ~3:1 due to the harem-style housing conditions at the SNPRC.

The ancestral kinship relationships have been documented for at least six generations (>30 years), allowing for use of all possible pair-wise relatedness coefficients in quantitative genetic analysis. A total of 2426 individuals are included and grouped into one unbroken extended pedigree. Of these, 2044 have been genotyped for ~300 short tandem repeat (STR) (microsatellite) loci (Rogers *et al.* 2000; Cox *et al.* 2006). Full sibships range in size from 2 to 12 individuals with a median of 5. Full information on the current state of the colony can be found on the SNPRC website: http://txbiomed.org/primate-research-center.

Skulls were collected at necropsy from 985 pedigreed baboons (see below). As the samples underwent a freezing process for their transfer to Washington University, destroying brain cells, we were unable to directly dissect their brains. However, CT scans were obtained, and 100 of these individuals had additionally been MR-scanned while alive (Kochunov *et al.* 2010; Rogers *et al.* 2010). We developed a method for virtual processing of CT images to create a well-textured virtual brain upon which biologically meaningful measurements could be reliably taken. Although we only used the CT measurements in analyses for the sake of consistency, we compared our CT endocast-based measurements with those taken on the overlapping MR scans to ensure accuracy and repeatability of data.

Endocast creation and landmark measurement

Over a period of 15 years, the heads of 985 animals were collected at necropsy and scanned at 0.6 or 0.7 mm with a 64-slice General Electric 3D CT scanner at the Mallinckrodt Institute of Radiology at Washington University. Virtual endocasts displaying brain topology were generated from the cranial CT scans by 3D image segmentation using the freeware program ITK-SNAP (Yushkevich *et al.* 2006). Images were processed with a standardized upper image threshold to minimize resolution differences, and seeds were arranged to maximize endocranial coverage. Three-dimensional landmark coordinates were collected on processed endocasts by manually placing points along specific brain sulci on the segmentation mesh using the Amira 5 program (Stalling *et al.* 2005). The total length along the 3D brain surface was captured for metric traits. The lengths of the following 10 sulci were collected on both the left and right hemispheres of the endocasts: arcuate rectus spur (arsp), central sulcus (cs), inferior arcuate rectus (iar), intraparietal sulcus (ips), lateral fissure (lf), lunate sulcus (lu), principal sulcus (ps), superior arcuate rectus (sar), superior precentral dimple (spcd), and superior temporal sulcus (sts) (Table 1; Supporting Information, Table S1; Figure 1). The quantitative genetic results presented here are of the average standardized length across hemispheres for each sulcus to reduce unnecessary complexity. Three additional

Table 1 Anatomical descriptions of landmark sulci

Trait code	Trait full name	Anatomical description of sulcus
arsp	Arcuate rectus spur	Possible posterior spur off of junction of arcuate rectus inferior and superior projections.
cs	Central sulcus	Major fold extending interiorly from midline of brain separating frontal and parietal brain lobes and curling rostrally or branching before reaching the lateral sulcus.
iar	Inferior arcuate rectus	Inferior branch of the arcuate rectus spanning from junction with arsp and/or sar to inferio-rostral edge of frontal lobe.
ips	Intraparietal sulcus	On lateral surface of parietal lobe spanning from inferio-frontal portion to intersection with lu just inferior to midline.
lf	Lateral fissure	Separates frontal and parietal lobes from temporal lobe and spans superior-posteriorly from superior-frontal edge of temporal lobe to approximate intersection with sts.
lu	Lunate sulcus	Separates parietal and temporal lobes from occipital lobe and spans inferiorly from intersection with ips just inferior to midline.
ps	Principal sulcus	Runs posterior-laterally from frontal edge of frontal lobe, ending just before intersection with iar.
sar	Superior arcuate rectus	Frontal portion of arcuate rectus running fronto-laterally from intersection with iar and/or arsp.
sts	Superior temporal sulcus	Runs superior-posteriorly from inferio-frontal edge of temporal lobe to approximate intersection with lf.
spcd	Superior precentral dimple	Possible short lateral fold in frontal lobe superior to arcuate rectus.
Larsp_yn		**Non-metric: presence/absence of left hemisphere arsp.**
Rarsp_yn		**Non-metric: presence/absence of right hemisphere arsp.**
Lcs_forked		**Non-metric: indicates whether the inferior tip of the left cs is forked or unforked.**
Rcs_forked		**Non-metric: indicates whether the inferior tip of the right cs is forked or unforked.**
Lspcd_yn		**Non-metric: presence/absence of left hemisphere spcd.**
Rspcd_yn		**Non-metric: presence/absence of right hemisphere spcd.**

Anatomical characterization of the position on the hemisphere, proximal, and terminal ends of the 10 metric and 6 non-metric cortical-folding traits examined on each brain hemisphere. Left and right hemispheres were collected separately on different days. Non-metric traits are in boldface type.

non-metric traits were collected on both hemispheres. These were whether the inferior tips of the cs were forked or unforked and the presence or absence (p/a) of the (left, L, and right, R) spcd and arsp (Table 1 and Table S2). The location of the two p/a sulci can be seen in Figure 1, as can an example of a cs with a forked inferior tip . All endocasts were double-measured for all identifiable sulci to ensure accuracy and quantify measurement error. Landmarks were collected on both hemispheres separately and double measurements were made at least 1 day apart to remove any potential measuring bias. An extremely conservative approach was taken in data collection such that when the sulcus was not clearly defined, the trait was logged as missing and omitted from analysis. This resulted in a considerable—but typical for endocast-based studies of brain topology (Cheverud *et al.* 1990)—amount of missing data. Analyses were thus done in a pair-wise fashion. Differences in sample sizes between traits can be seen in Table 2.

Covariate screening

Prior to quantitative genetic testing, pertinent covariates were screened for an effect on each phenotype, and the mean effect of significant covariates ($P < 0.05$) was regressed out. All quantitative genetic analyses were conducted on the resultant residuals. This removes concerns about confounding genetic results with correlated variation in other traits while preserving the natural variation in our phenotypes. Covariates that were not significant for traits were not included in the genetic analysis. Covariates screened for were age, sex, the interaction of age and sex (age $\times$ sex), age^2, and cranial capacity (CC), as has been done in previous studies on this population (Kochunov *et al.* 2010; Rogers *et al.* 2010). Table 2 documents which covariates were significant for each of the traits. An extended description and rationale for each covariate is provided in the Supporting Information.

Quantitative genetics and creation of correlation matrices

Heritability (h^2) estimates and genetic correlations were calculated using the Sequential Oligogenic Linkage Analysis Routines (SOLAR) software package (Almasy and Blangero 1998). SOLAR, which is thoroughly described elsewhere (Almasy and Blangero 1998), implements a maximum-likelihood-based algorithm and uses variance component methods to determine heritability and pair-wise genetic correlations assuming a Gaussian distribution. Non-metric traits were analyzed using an algorithm tailored to discrete phenotypes (Duggirala *et al.* 1997; Williams *et al.* 1999). This involves a liability threshold model for dichotomous traits. Variance component methods are useful for large, complex pedigrees. SOLAR takes into account all relatedness coefficients between individuals to determine an identity by descent matrix that can then be used to map traits. The covariance matrix, Ω, for an extended pedigree is $\Omega = 2\Phi\sigma^2_g + I\sigma^2_e$, where the kinship matrix, Φ, gives all pair-wise kinship coefficients; σ^2_g is the genetic variance due to additive genetic effects; σ^2_e is variance from individual-specific environmental effects; and I is an identity matrix. The genetic matrix created for this study can be found in Table S3.

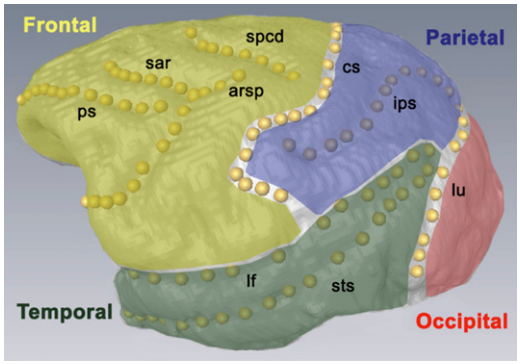

Figure 1 Brain-fold traits examined by brain area. Fully annotated left hemisphere of a representative CT-based virtual endocast showing placement of all 10 metric sulci and their partitioning into anatomical lobe regions. Landmark points used in data collection are seen as dots along the sulcus curvature. Anatomical lobe region assignment is designated by placement of sulcus and name.

The matrix of phenotypic variation (Table S4) was created from the covariate-corrected data using the R statistical package (R Core Team 2012). Prior to cross-domain matrix comparison, sulci were screened on the two hemispheres separately in case they exhibited different modular structures (Cheverud *et al.* 1990; Hutchison and Cheverud 1992; Sun *et al.* 2005; Im *et al.* 2010), but both left and right sides displayed the same patterns. The two were thus centered and averaged to add to the sample size, reduce unnecessary noise, and maintain compatible dimensionality of all matrices for comparison.

An anatomic similarity matrix was created based on sulcus locations on the cerebral cortex (Table S5). Lobes were partitioned at their traditionally defined borders (Figure 1). The following rubric was followed to assign values in the matrix: if the two sulci in question intersect, a value 0.9 was assigned; if sulci are adjacent, 0.6; in adjacent lobes but have other folds between them, 0.3; and in nonadjacent lobes, 0.1. The only sulcus that has a different number value assigned from the ones listed is spcd compared to other frontal sulci. Since these folds are in the same lobe but are not adjacent, a value of 0.5 was assigned.

Markov *et al.* (2014) quantify the degree of connectivity between 97 brain regions in *Macaca fascicularis*, another member of the tribe Papionini, by counting the number of axons physically connecting different brain regions. We used these data to create a connectivity similarity matrix for landmark sulci, with connectivity amount between pairs of sulci ranging from 0 (no axons connecting regions) to 1 (self) (Table S6). As the raw matrix was not symmetric due to differences between numbers of axons projecting from source to target *vs.* from target to source, a compromise matrix of the average between these two measures was used. Some regions were characterized only as an axon source and not a target, in which case this measure alone was used in downstream analyses.

A developmental matrix was created from data published by Sawada *et al.* (2012) illustrating the ontogeny of cortical development in *M. fascicularis* (Sawada *et al.* 2012) (Table S7). We created a distance matrix between sulci based on their relative times of developmental emergence in days from conception. Sulci emerge between embryonic days 70 and 135. This distance matrix was then converted into a similarity matrix by taking the reciprocal of the data for the sake of comparison with other matrices in analyses. In designing this project, we chose baboon sulci that are orthologous to those present in the macaque specifically for comparison with literature-based data. Macaques are the most closely related primate to baboons that have been extremely well described in terms of brain development and functional connectivity. It is reasonable to suspect that sulcal embryonic timing and connectivity would be similar between these two species due to their similar brain structures and evolutionary and genetic relatedness. Our Mantel comparisons represent a theoretical proof-of-concept test, so slight differences in patterns between these Papionini species will not seriously impact interpretation.

Since genetic and phenotypic correlations are estimates of the true values and thus have error incorporated into them, it is necessary to assess the degree of repeatability within the correlations to determine the true significance of the patterns of matrix similarity detected. In general, a matrix's repeatability (t) is the proportion of the variance observed in measurements that is due to true population variation as opposed to error variation. Since there will always be some error incorporated into estimates, if two population matrices are perfectly correlated, the largest correlation value that can be observed between them will be a function of both of their repeatabilities. Thus, our Mantel matrix correlations could seem low when considered independently, but could actually be approaching the maximum possible value that can be attained, given the degree of error in estimates. For this reason, both the Monte-Carlo matrix correlation value, its P-value, the maximum t value attainable, and the ratio of the observed r over the maximum t (how close to perfectly the matrices actually are correlated, with error) are provided here. Repeatability was calculated for both estimated matrices as previously described (Cheverud 1996). As we cannot calculate t for the theoretical matrices (developmental, connectivity, anatomical lobe), their maximum possible Mantel correlation value was conservatively assumed to be 1.

Modularity and cluster analysis

We used Mantel's test to identify the degree of structural similarity between phenotypic, genetic, connectivity, and developmental matrices. Mantel tests assess the similarity of the pattern of variation present in compared matrices and provide an estimate of the probability that the observed structural similarity could be observed under a null hypothesis of no similarity. Mantel tests were done using the ade4 package of R (Dray and Dufour 2007). In all Mantel tests, 9999 randomizations were performed. Mantel tests were quite robust to slight variations in the construction of literature-based matrices. Each comparison of matrix pairs conducted here addressed a distinct biological hypothesis. For example, the genotype–phenotype Mantel comparison tested the hypothesis

Table 2 Trait heritability results

Sulcus	h^2	h^2 SE	h^2 *P*-value	*n*	Significant covariates	Average length	*Vp*	*Va*
arsp*	0.354	0.081	<0.001	675	Age^2, CC	15.9	5.911	2.092
cs*	0.281	0.076	<0.001	621	Sex, CC	95.84	8.497	2.388
iar	0.053	0.072	0.178	670	Age, age-by-sex, age^2, CC	60.2	25.418	1.347
ips*	0.133	0.075	0.002	491	Age, age-by-sex, CC	75.72	12.936	1.721
lf*	0.235	0.103	<0.001	429	Sex, CC	99.34	18.579	4.366
lu*	0.197	0.121	0.01	360	Sex, CC	75.73	10.836	2.135
ps*	0.512	0.113	<0.001	541	Age, sex, age-by-sex, CC	59.49	5.385	2.757
sar	0.053	0.048	0.077	574		27.504	18.635	0.988
spcd	0.01	0.045	0.406	507		35.793	17.301	0.173
sts*	0.114	0.09	0.036	359	Sex, age, age-by-sex, age^2, CC	115.86	15.184	1.731
Larsp_ yn	**—**		**0.5**	**627**		**0.812**		
Lcs_forked*	**0.134**	**0.097**	**0.021**	**606**		**0.606**		
Lspcd _yn	**—**		**0.5**	**663**		**0.905**		
Rarsp _yn*	**0.129**	**0.070**	**0.003**	**737**		**0.826**		
Rcs_forked	**0.065**	**0.060**	**0.076**	**669**		**0.590**		
Rspcd_ yn*	**0.15**		**0.019**	**747**		**0.876**		

Heritability (h^2) estimates, heritability standard errors (SE), and significance (*P*) calculated for each of the 10 metric sulcal length measures (boldface) and 6 nonmetric traits (roman). Significant results are indicated with asterisks by the trait name. Covariates that emerged as significant for that trait during screening and the trait sample size are listed. Age-by-sex is the interaction between age and sex; CC is cranial capacity. Sulcus average lengths are in millimeters. "Average length" reports for nonmetric traits are the frequency of occurrence of the presence of that trait for arsp and spcd phenotypes and the frequency of forked cs. *Vp* is the phenotypic variation for traits; *Va* is the additive genetic variation for traits.

that there is genetic control over trait variation patterns, while anatomy–development tested the hypothesis that a fold's position on the endocast could be used to predict how early in embryonic development the sulcus would appear. Since these comparisons address different hypotheses and we are interested in each hypothesis separately, our Mantel comparisons do not represent a situation where there is need to control for multiple testing as they do not constitute a set of tests of the same hypothesis.

Hierarchical cluster analysis was performed on the phenotypic and genetic matrices to visualize the structure of variation using an agglomerative approach (Hartigan 1975, 1985). These correlation matrices were converted into a distance matrix format for these purposes. A variety of methods (average, Ward, complete linkage) were used to determine the most robust cluster arrangement, which generally was represented by the average linkage method. For this reason, only average linkage clustering results are reported in this article.

k-Means testing was conducted using the two traditional algorithms (Hartigan and Wong 1979; Lloyd 1982) to independently determine the correct number of clusters and assign sulci to clusters based on their phenotypic and genetic relationships. *k*-Means is a heuristic criterion rather than a statistical approach, so there is no discrete cutoff point for clustering. Rather, it can be used to inform and corroborate results of the hierarchical clustering. The "elbow" in the *k*-means results was identified by examining the improvement of explanation of variation with each additional cluster. The greatest improvement to the ratio of the between-cluster sum-of-squares to the total sum-of-squares after which there was minimal improvement was determined to be the preferred value for *k*. Both algorithms agreed on the number of clusters for both matrices.

QTL mapping

QTL mapping was used to pinpoint chromosomal regions affecting variation in all metric cortical phenotypes. QTL analysis has a very low rate of type I error, but is limited in its ability to identify genes of small effect. We do not presume that we can identify all the loci affecting cerebral gyrification in this study. However, implicating any genomic regions as affecting gyrification is a substantial step forward in this incipient research field. QTL analysis was conducted using SOLAR, which minimizes the false-positive rate of QTL peaks by limiting results to true relatedness as opposed to simply sharing an allelic state. SOLAR was also used to calculate LOD scores across the baboon genome. A LOD score indicates the ratio of the likelihood of obtaining a signature of linkage if the marker and locus are indeed linked *vs.* the likelihood of obtaining the observed result by chance. The SNPRC has created an extensive whole-genome microsatellite-based linkage map for this population based on genotypes from 284 marker loci that are 2354 cM long (Rogers *et al.* 2000; Cox *et al.* 2006). Markers were selected to be as evenly spaced throughout the genome as possible, with an average intermarker distance of 8.9 cM and average heterozygosity of the microsatellite loci of 0.74.

LOD score thresholds were calculated on both chromosome-wise and genome-wide scales in SOLAR using a modification of the approach suggested by Feingold *et al.* (1993), controlling for the overall false-positive rate, given the finite marker locus density in the baboon genome map and pedigree complexity. This modification improves the accuracy of results for continuously varying quantitative traits in complex pedigrees with multiple relative classes. QTL power calculations for a pedigree of this constitution were conducted during linkage map creation. In simulations with 1000 replicates at each QTL-specific effect size, there was determined to be 80% power to detect a significant QTL responsible for as small as 5.5% of the total phenotypic variance (Lander and Kruglyak 1995; Almasy and Blangero 1998). For this, simqtl procedures were implemented, modeling a quantitative trait

Table 3 Mantel testing results

Comparison	Monte-Carlo correlation	*P*-value	Maximum *t*	Ratio
Genetic–phenotypic*	0.390	0.003	0.563	0.693
Phenotypic–development	0.066	0.254	0.948	0.069
Phenotypic–connectivity	−0.046	0.616	0.948	−0.049
Phenotypic–anatomy	0.202	0.094	0.948	0.213
Genetic–development	−0.096	0.728	0.335	−0.286
Genetic–connectivity	−0.121	0.755	0.335	−0.361
Genetic–anatomy	−0.078	0.700	0.335	−0.234
Anatomy–development*	0.289	0.048	1.000	0.289
Connectivity–development*	0.288	0.040	1.000	0.288
Anatomy–connectivity*	0.511	<0.001	1.000	0.511

Monte-Carlo matrix correlation, the *P*-value of the test, the maximum possible *t* value attainable with error, and the ratio of the estimated matrix correlation to the maximum *t* are shown for all domains compared. The ratio indicates the corrected matrix correlation value. The four significant comparisons are indicated by asterisks.

that is influenced by a single, bi-allelic QTL with a residual additive genetic effect due to polygenes. To control for genome-wide false-positive QTL hits, the expected LOD scores estimated for a QTL with a specific effect size between 0.01 and 0.05 were calculated. These values were used to determine the thresholds for genome-wide significance at LOD = 2.75 and for suggestive evidence of linkage at LOD = 1.53 at $\alpha = 0.05$ with this pedigree configuration. Such a significance threshold corresponds to the expected type I error rate of once per 20 whole-genome linkage screens. Power tests were based on the 840 baboons that were part of the pedigree at that point in time. All 840 animals are phenotyped and genotyped in this study. These power calculations thus represent a minimum estimate of the true power for QTL detection of our current, expanded data set.

Results

Endocast validation

Due to a very close ontogenetic relationship between brain shape and the bones of the skull, sulci are visible as ridges on the endocranial surface in Old World Monkeys, making endocasts useful for analysis of cortical features (Moss and Young 1960; Falk 1986, 1987; Enlow 1990; Bruner 2003; Holloway *et al.* 2005). The utility of CT-based virtual endocasts for studies of primate brain evolution, including in examination of cortical-folding features, has been validated in both anthropology and paleoneurobiology (Zollikofer *et al.* 1998; Bruner 2003, 2004, 2007, 2008; Zollikofer and de León 2005; Carlson *et al.* 2011; Balzeau *et al.* 2012; Falk 2014; Kobayashi *et al.* 2014). Our measurements taken on these CT scan-based virtual endocasts showed extremely high repeatability (average = 93%), implying reliable and consistent data collection. Furthermore, we found an exceptionally tight correlation between the sulcal length measurements taken on CT endocasts compared with those from 100 magnetic resonance imaging scans of the same individuals (average = 95%). This verifies the biological meaningfulness of endocast cortical measurements; these CT-based virtual endocasts consistently and reliably capture the sulcal shape variation of the true cortex. See Supporting Information for details on repeatability calculations.

Heritability

There is a moderate genetic basis to variation in both the metric and non-metric cortical sulcal traits measured in this population. The average of sulcal length heritability (h^2) for all metric traits with a sample size great enough to reach significance was 0.26, which is within the normal range for morphological traits (Visscher *et al.* 2008). The lengths of 7 of the 10 landmark sulci were significantly heritable—all but iar, sar, and spcd. Of the covariates included in the analyses, cranial capacity was typically significant, with age, sex, and their interactions occasionally being so. Table 2 shows the h^2 results for all traits, their individual significance levels, significant covariates, and sample sizes.

Three of the non-metric traits had significant h^2 estimates: Lcs_forked, Rarsp_yn, and Rspcd_yn. The average significant h^2 calculated for non-metric traits was 0.14. Non-metric traits were controlled for the same covariates as metric to ensure that h^2 corresponded only to genetic variation of the phenotype in question. These h^2 estimates are likely underestimates, as any error in the data would detract from the true value; here, ~5–10% of trait variation was due to measurement error. The difficulty in assessing heritability of sulcal pattern has been noted in previous studies (Winterer and Goldman 2003).

Mantel testing and cluster analysis

Matrix repeatabilities (*t*) were calculated for the two matrices created from our data: phenotypic and genetic. The *t*-value was 0.34 for the genetic matrix and 0.98 for the phenotypic. All permutations between distance matrices created from correlation matrices were compared to test different biological hypotheses about cortical modularity, development, and connectivity. Four of these comparisons indicated statistically significant similarity between matrix pairs (Table 3). The four statistically similar matrix comparisons, listed with their Monte-Carlo observed matrix correlations and *P*-values, were genetic–phenotypic ($r = 0.39$, $P = 0.003$), anatomic–developmental ($r = 0.29$, $P = 0.048$), connectivity–anatomic ($r = 0.51$, $P = <0.001$), and connectivity–developmental ($r = 0.29$, $P = 0.040$). Taking into account the fact that 0.563 is the maximum matrix correlation that could be observed using our data set between the phenotypic and genetic

matrices in light of the matrix repeatabilities, the corrected genetic–phenotypic matrix correlation is 0.693.

Hierarchical clustering and *k*-means methods were used to determine the appropriate module breakdown of the phenotypic and genetic relationships. Agglomerative hierarchical clustering links individual traits to one another iteratively to create a network. *k*-Means testing provides an estimate of the quality of fit in grouping *n* traits into *k* clusters. Table 4 contains the results for *k*-means examination of phenotypic and genetic data in tests from $k = 2$ to $k = 7$. Clustering analyses of the phenotypic correlations suggested three clusters of approximately equivalent size (ps, iar, sar; cs, lu, arsp; and spc, ips, lf, sts) (Figure 2, A and B). Although there was not an obvious elbow for the phenotypic data, the amount of improvement drops most dramatically after three clusters (Table 4). For this reason, combined with the fact that partitioning phenotypic variation into three modules additionally is the most biologically realistic outcome, $k = 3$ was determined to be the correct cluster number for the data. All clustering methods agreed on both cluster number and assignment of traits into groups at $k = 3$.

The clustering results for *k*-means and hierarchical clustering were both most compatible with there being four genetic modules (Table 4 and Figure 2, C and D). *k*-Means testing and hierarchical cluster analysis did not perfectly agree on the precise assignment of sulci into clusters due to the larger standard errors in genetic data, but the most consistent results across all algorithms are presented here. These clustering results are shown as produced by the average linkage criterion for hierarchical clustering and the Hartigan–Wong method for *k*-means testing. For consistency, phenotypic results are plotted using these methods as well.

QTL mapping and genetic architecture

One QTL passed the stringent genome-wide threshold, while 11 additional peaks passed the suggestive LOD threshold. All peaks passing either threshold are documented in Table 5. Peaks prioritized for follow-up were selected based on the criteria of LOD score, peak width, and the presence of compelling positional candidate genes. To control for the unlikely event that a false peak managed to break the lower threshold, only the highest peaks were selected for further examination (Figure 3; Table 6).

The highest peak obtained in the study, breaking the stringent genome-wide threshold, was for trait lu and appeared on baboon chromosome 3 (Figure 3A). This QTL contained two gene clusters associated with well-characterized neurological disorders: Williams and Down syndromes. Williams syndrome in particular is specifically associated with abnormal gyrification. Specifically, the Williams syndrome-associated genes within the confidence interval for chromosome 3 were the following: Williams Beuren Syndrome Chromosome Region 22 (*WBSCR22*), Frizzled Family Receptor 9 (*FZD9*), Bromodomain Adjacent to Zinc Finger Domain 1B (*BAZ1B*), and MLX Interacting Protein-Like (*MLXIPL*). The genes within the positionally relevant Down syndrome gene cluster were the following: Glutamate Receptor Ionotropic Kainate 1 (*GRIK1*), Oligodendrocyte Lineage Transcription Factor 2 (*OLIG2*), Regulator of Calcineurin 1 (*RCAN1*), Single-Minded Family bHLH Transcription Factor 2 (*SIM2*), Dual-specificity Tyrosine-(Y)-phosphorylation Regulated Kinase 1A (*DYRK1A*), Beta-site APP-Cleaving Enzyme 2 (*BACE2*), and S100 Calcium Binding Protein B (*S100B*) [National Center for Biotechnology Information (NCBI) genome database, http://www.ncbi.nlm.nih.gov/genome/].

Table 4 Cluster number determination from *k*-means testing

k	Phenotypic	Genetic
2	44.8	36.7
3	61.5*	47.6
4	71.8	61.9*
5	76.0	69.3
6	83.4	79.2
7	85.2	83.3

Results for *k*-means testing of phenotypic and genetic correlation matrices using the average of the Lloyd (1982) and Hartigan and Wong (1979) algorithms. Hypothesized cluster number is the *k*-value input into the heuristic. Numbers reported for the phenotypic and genetic matrices are the average of the two algorithms' results for the ratio of the between-groups sum-of-squares to the total sum-of-squares. The point at which the curve was determined to have its "elbow" is indicated with an asterisk.

The second-highest peak appeared on baboon chromosome 12 (Figure 3B). It was significant for numerous traits, indicating pleiotropic effects and its widespread role in cortical-folding development. This QTL additionally contained a handful of compelling candidate genes that make it of interest for further investigation. These genes were the following: Delta/Notch-like EGF Repeat Containing (*DNER*), Neuromedin U Receptor 1 (*NMUR1*), EF-Hand Domain Family Member D1 (*EFHD1*), GRB10 Interacting GYF Protein 2 (*GIGYF2*), and Neuronal Guanine Nucleotide Exchange Factor (*NGEF*), and all have also been implicated in affecting brain development or neuronal function.

The genome-wide distribution of QTL peaks illustrates a complex genetic architecture underlying cortical gyrification in primates. First, a number of different traits mapped to the same chromosomal position. This is an indication of QTL pleiotropy, as the same gene or suite of genes present at the identified location is likely contributing to variation in the multiple significant phenotypes. An example of QTL pleiotropy on baboon chromosome 12 can be seen Figure 4. Further tests of the observed pleiotropy in this region were run in an effort to provide additional support for pleiotropy over coincident linkage. Analyses comparing QTL-specific ρ_G (additive genetic correlation) sets for polygenic traits did not reach statistical significance, but were near-significant ($P \approx 0.08$) in the overlap region. This supports there being borderline-significant QTL-specific additive genetic correlations for putative pleiotropic traits and argues against the conclusion that these findings are due simply to coincident linkage. Larger pairwise trait sample sizes would be needed to boost ρ_Q values to the $\alpha = 0.05$ level.

The data additionally show indications of polygeny, the situation where one trait is affected by multiple genes. Nearly all traits mapped significantly to more than one position in

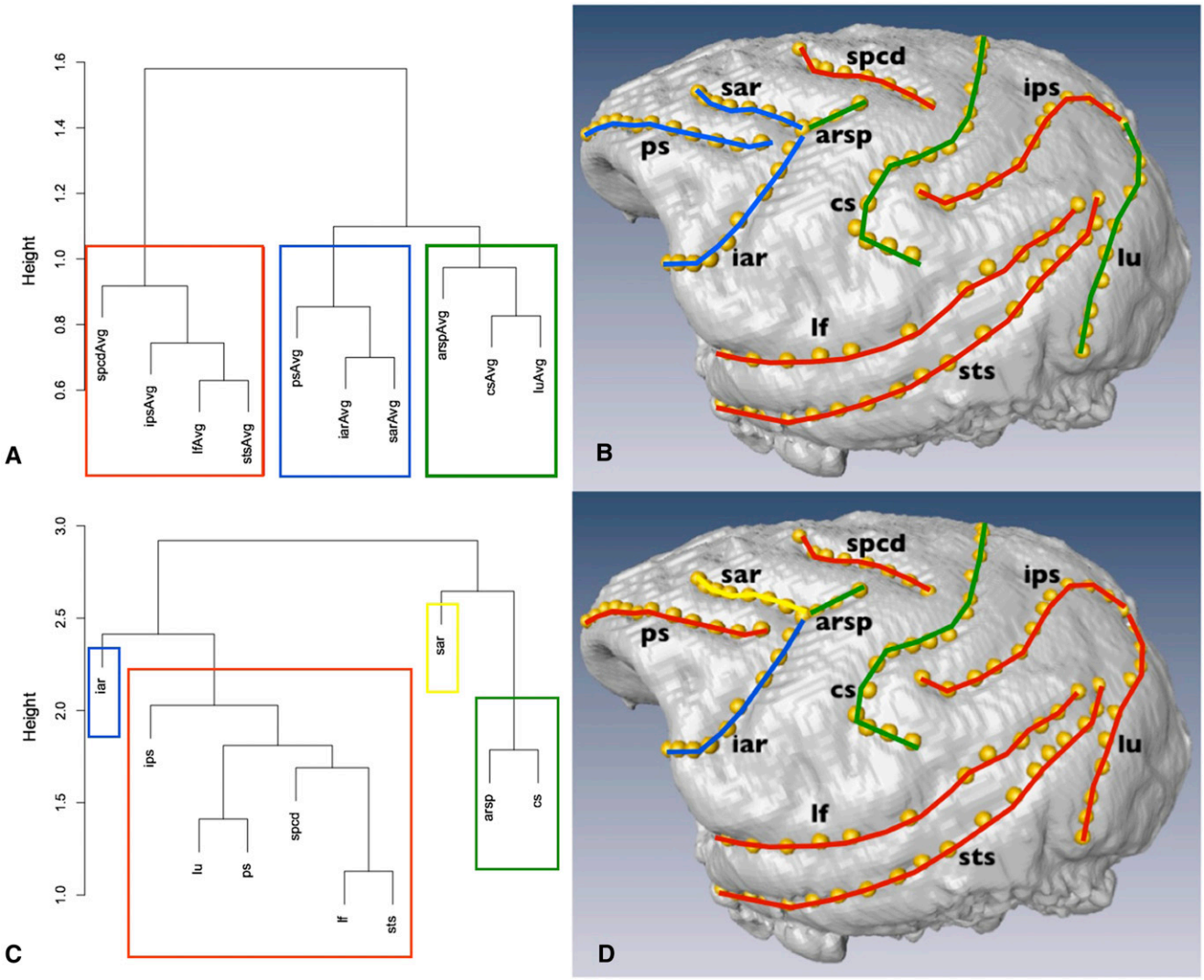

Figure 2 Sulcus module assignments for phenotype (A and B) and genotype (C and D). Hierarchical clustering dendrograms (left) were created using the average linkage method. Colored boxes illustrate the module borders determined by *k*-means testing using the Hartigan–Wong algorithm. Annotated endocasts (right) visualize sulcus module assignment. Module color is retained between phenotype and genotype.

the genome, supporting the postulate that most cortical phenotypes are controlled by a number of genes of small effect (Mackay 2001; Cookson *et al.* 2009) rather than a single gene of large effect determining gyrification pattern. The average number of significant QTL for those traits with at least one significant peak was 1.71, indicating that if traits were able to pass a threshold once, it was not uncommon for them to do so at least one more time. Often, subthreshold peaks were also visible, indicating the likely presence of additional affected traits or causative loci that did not pass the extremely conservative thresholds required for multiple comparisons.

Discussion

Quantitative genetics

It should first be noted that there are many interesting phenotypes associated with cortical morphology. In the current study, we aim to address the general question of the overall amount of gyrification across brain hemispheres by examining variation in the length of specific landmark sulci. Although these sulci were chosen to characterize a large portion of the cerebrum, there are many additional traits of interest that could be investigated further in future studies (*e.g.*, depth of sulci, additional sulci not included here) that would complement these results.

The average significant heritability of 26.1% for metric traits falls into the range typical for morphological traits. This supports the hypothesis that brain cortical gyrification is not random but instead is under a significant, moderate degree of genetic control with additional environmental effects. Significant results even after removing the effects of cranial capacity and other size correlates support prior indications (Rogers *et al.* 2010) that gyrification has at least partial genetic control independent of brain volume. Gyrification thus has its own evolutionary history in primates and has potentially

Table 5 QTL mapping results

Baboon chromosome	Trait	LOD score	Human ortholog	Locus (cM)	Proximal CI (Mbp)	Distal CI (Mbp)
3	arsp	1.806	7_21	120	41	125
3	lu	3.187	7_21	39	14.2	33.4
4	arsp	1.688	6	65	87.6	128.5
5	iar	1.699	4	133	154.5	180
6	arsp	1.649	5	85	9	14.6
6	cs	2.472	5	39	9	76.7
8	arsp	1.631	8	50	10	40
9	ps	2.378	10	40	26	69
11	lu	1.680	12	56	44	100
12	ips	1.565	2q	145	132	140
12	lu	2.162	2q	127	226.5	233

Locations and widths of all QTL peaks passing suggestive (LOD = 1.53) or stringent (LOD = 2.75) thresholds using the full population. QTL width confidence interval (CI) boundaries were determined by the one-LOD drop point on either side of the peak marker. Linkage map locus positions are in centimorgans. CI basepair positions are in million basepairs.

been influenced by natural selection separately but in tandem with forces selecting for larger brains.

Non-metric traits were also found to have significant heritability, but show a lower degree of genetic control over phenotypic variation. This implies that the finer details of shape within cortical-folding features are under some genetic control, but are more influenced by environmental effects than are the lengths of sulci. The fine-grained shape of sulci is apparently less genetically constrained than their length or overall degree of gyrification.

Modularity

The distribution of variation elucidated interesting trends regarding the boundaries of modules across different biological domains. There was a close relationship between genetic and phenotypic partitioning of brain features, consistent with our finding of genetic control over variation in sulcal length traits. This pattern is also consistent with past natural selection resulting in effective morphological integration of cortical traits. A strongly modular system of variation imposes constraints on morphological evolution (Cheverud 1984, 1995, 1996; Wagner *et al.* 2007; Klingenberg 2008; Gómez-Robles *et al.* 2014) as correlation among traits reduces the amount of variation available to selection along some morphological dimensions. Although constraints are often assumed to restrict the response to natural selection, some degree of constraint over the direction of evolution can actually lead to increased rates of adaptation in specific directions (Wagner and Altenberg 1996), and canalization of variance prevents traits from wandering into deleterious regions of phenotypic space. When variation in functionally related traits is restricted to a common set of genes, the coordinated evolution of these traits will result in a functionally compatible set of outcomes (Wagner 1984, 1988, 1996; Gibson and Wagner 2000). Restricting phenotypic variance into modules also allows systems to evolve patterns of correlation that facilitate future alteration of evolutionary traits through the convergence of genetic and functional modules (Cheverud 1996; Wagner 1996). The similarity of variation structure in genetic and phenotypic matrices thus illustrates the selective grouping of traits into related units in these two domains, providing a ready framework for future adaptive morphological change and an evolutionarily beneficial situation of increased morphological integration for traits that need to be functionally compatible with one another in an organism's life.

The similarity in matrix variation structure between the anatomical location of the sulci and the day on which the sulcus first emerges during development parallels ontogenetic findings that the brain typically develops the primary and most deep-set folds first during development, with secondary folds developing next, and superficial wrinkles and projections off of the primary folds developing last (Huang *et al.* 2009; Sawada *et al.* 2012). The bulk of the primary folds are located toward the central region of the brain (lf, sts, cs), followed by the back of the brain (lu, ips), and finally the frontal folds (ps, spcd, iar). Superficial projections (arsp, sar) come last in development.

The final two significant results found from Mantel testing together provide indirect support for the propositions of the Van Essen model. The finding that strong similarity exists between the patterns of variation in connectivity and anatomical location of the sulci implies that connectivity is indeed paralleled by anatomical proximity (Markov *et al.* 2011). This theoretical result supports the mathematical models proposed concerning tension-based methods of cortical fold development (Mota and Herculano-Houzel 2012; Bayly *et al.* 2013) in an additional primate system. Moreover, the finding that there is significant similarity between the pattern of variation in connectivity and development hints at the interplay between the two factors in cortical formation. Tension imposed by white matter affects the emergence of sulci such that those dividing the most basal functional areas appear first in development (Kaymaz and Van Os 2009). Our results suggest that subsequent wrinkles and dimples might arise as the neural network becomes pruned and strengthened over the course of brain ontogeny. The modular patterns detected in these three domains therefore fall in line with the expectations of sulcal development theories based on axonal mechanical tension, rather than competing hypotheses for the origin of gyrification.

Turning to the structure of modules across biological domains, the first principal component for trait phenotypic

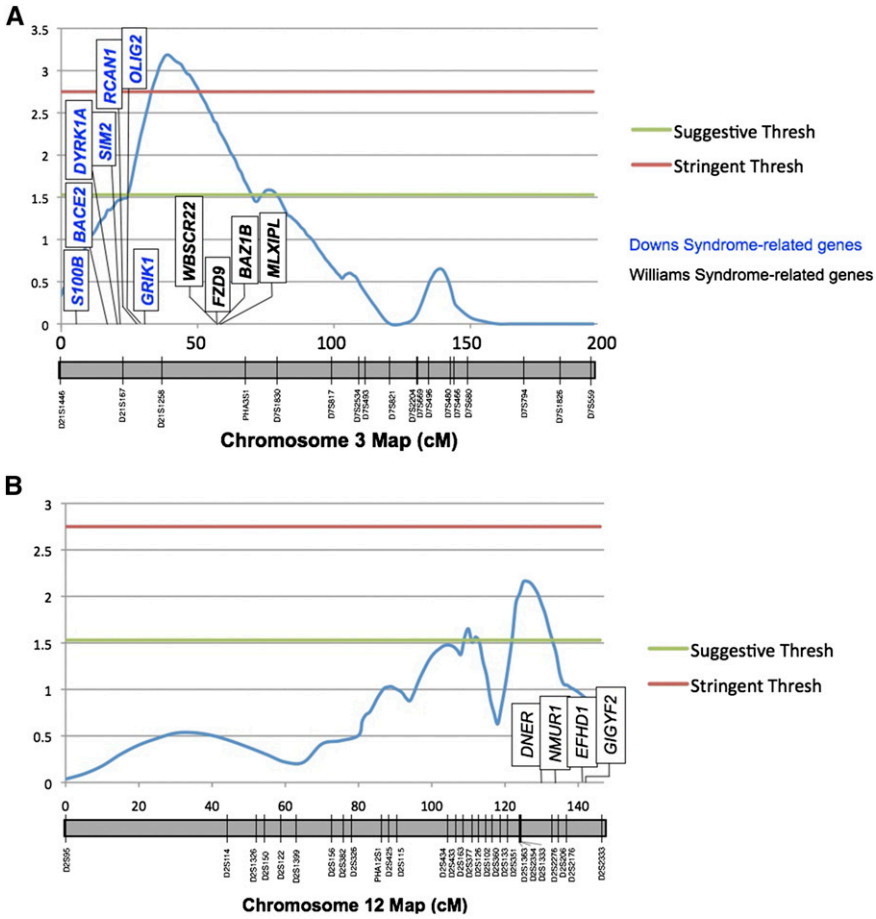

Figure 3 Highest-priority QTL peaks. QTL maps for the lunate sulcus (lu) on (A) baboon chromosome 3 (orthologous to human 7_21) and (B) baboon chromosome 12 (orthologous to human 2q). Linkage map is shown in centimorgans. Marker names and positions are documented on the chromosome schematic along the *x*-axis. Location of candidate genes within the peak confidence intervals are labeled in boxes. Horizontal lines indicate suggestive and stringent genome-wide thresholds.

variation, as determined by cluster analysis, roughly appears to correspond to orientation along the cortex. If we examine the hierarchical clustering network for the phenotypic data, the first sulcal group spans the frontmost portion of the endocast (Figure 2, A and B, blue). The next sulcal group that emerges has similar, roughly vertical orientations (Figure 2, A and B, green). The third main sulcal cluster consists of the sulci that cover the horizontal plane's inferiofrontal–superioposterior axis (Figure 2, A and B, red). This overall grouping structure was very robust to different testing methods.

Despite best fitting with four modules rather than three, the genetic matrix clustering results (Figure 2, C and D) show a similar overall trend to the phenotypic pattern, as would be expected based on the similarity between these two matrices in the distribution of variation across phenotypic space as shown by Mantel testing. Specifically, the general trend of sulcal orientation across the cortex seems to hold for module determination, but with sar falling out into its own cluster and lu collapsed into the broader red group. This pattern is similar to that seen in the phenotypic matrix, and an examination of lower values of *k* for the genetic matrix matches phenotypic results even more closely. The borders to genetic modules in the brain have major implications as to the potential constraints imposed on the future evolutionary alteration of brain topology, including on selection acting on other biological domains. There could be selection focusing on developmental or connectivity phenotypes, but it is the DNA, the molecular substrate of evolution, that will reflect such pressures across generations.

Genetic architecture

The distribution of QTL peaks across the genome highlights the complex genetic architecture underlying cortical gyrification. We found multiple QTL peaks during linkage mapping, implying that numerous genes of small effect influence folding rather than a single gene of large effect. Additionally, through the recurrence of peak regions for distinct traits and the detection of numerous peaks for individual traits, we note both pleiotropy and polygeny for cortical features in this population.

One notable example of pleiotopy is for the traits of lu and sts on baboon chromosome 12 (Figure 4). This region is interesting for fine-mapping follow-up and candidate gene investigation, as a gene or gene cluster here seemingly has a relatively large effect on a number of different cortical sulci. It is interesting to note that these traits are all located toward the posterior portion of the cerebrum, behind the central sulcus (Figure 1). This could be an indication of these brain features sharing a common developmental pathway.

Table 6 Candidate genes contained within peak region of the top two QTL

Trait	LOD score	Baboon chromosome	Human chromosome	Peak locus (cM)	Width (cM)	Candidate genes
lu	3.18	12	02q	126	16	*DNER*, *NMUR1*, *EFHD1*, *GIGYF2*, *NGEF*
lu	2.16	3	07_21	39	32	Williams syndrome gene cluster (*WBSCR22*, *FZD9*, *BAZ1B*, *MLXIPL*); Down syndrome-related genes (*GRIK1*, *OLIG2*, *RCAN1*, *SIM2*, *DYRK1A*, *BACE2*, *S100B*)

Peak characteristics for the two QTL of highest priority, including candidate genes within confidence interval regions, are given. Listed genes have been empirically implicated in affecting neurological development and/or function.

Candidate genes

A number of intriguing candidate genes are located in the peaks of highest interest (Table 6). The top two peaks identified in this study were for lu on baboon chromosomes 3 and 12. The peak for lu present on baboon 12 is of note due to its threshold-breaking recurrence for multiple cortical features (Figure 4). The region additionally contains a number of candidate genes of interest (Table 6) that have all been empirically shown to affect neuronal development and/or function in primates and are highly conserved across vertebrate species. There are therefore direct reasons to suspect that these genes could affect brain-fold development and adult cortical topology.

The second peak of interest was on baboon chromosome 3 (Table 6 and Figure 3A). This QTL attained LOD = 3.18, the highest score reached in this study, and was the only peak to break the rigorously stringent threshold for detecting genome-wide significance. Furthermore, it contains two extremely intriguing gene clusters with relevance to cortical gyrification and brain function (NCBI genome database). One gene suite on the periphery of the peak contains four genes that have been shown to be involved in Williams syndrome, a genetic disorder associated with abnormal cortical-folding patterns (Bellugi *et al.* 2000; Korenberg *et al.* 2000). A second gene cluster, located directly under the peak's apex in the baboon chromosomal region orthologous to human chromosome 21, contains a cluster of Down syndrome-associated genes. All of these positional candidate genes have been empirically shown to affect nervous system development and function (Abdul-Hay and Sahara 2012; Hirata and Zai 2012; Lu *et al.* 2012; Streitbürger *et al.* 2012; Bhoiwala *et al.* 2013; Chatterjee and Dutta 2013; Hijazi *et al.* 2013). The genomic stretch containing this gene cluster has even been dubbed the "Down syndrome critical region" of human chromosome 21, making it a strong contender for playing a major role in brain development. The presence of these two gene clusters within this single peak makes this baboon chromosome 3 QTL of highest priority for future fine-mapping studies and candidate gene evaluation.

At this stage in our analyses, we have honed in on chromosomal regions of interest that are extremely likely to be involved in affecting baboon cortical folding. This provides a solid starting point for future work targeting specific positional candidate genes. To get from the QTL down to the quantitative trait gene (QTG), one would have to associate specific variants within genes of interest with variation in brain traits. Following such a step with functional testing of positional candidates would provide a robust demonstration of their effect on brain development and morphology.

Conclusions

Here, using CT-scan-based virtual endocasts from a pedigreed baboon population of unprecedented size for such research using nonhuman primates ($n = \sim 1000$), we have characterized the heritability of cortical gyrification features, finding significant heritability for nearly all metric traits. Non-metric shape features additionally exhibited significant

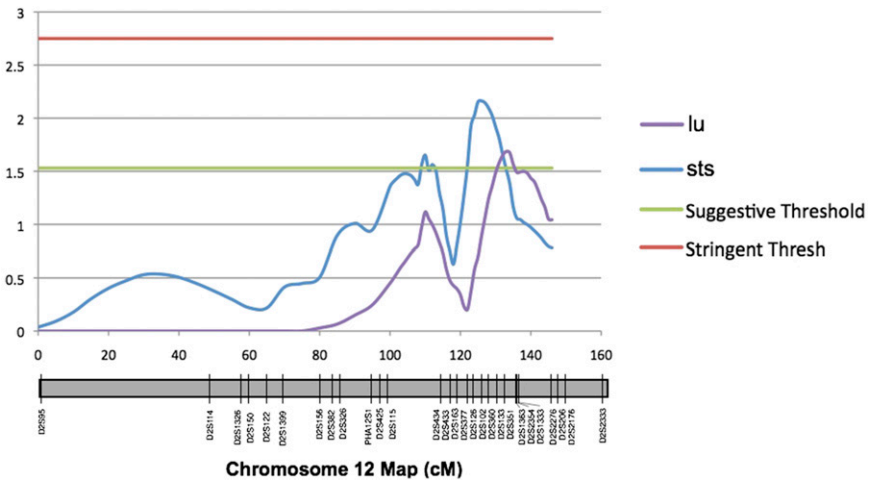

Figure 4 Example of QTL pleiotropy. QTL map of baboon chromosome 12 (orthologous to human 2q) showing positional overlap of peaks for two distinct traits: lu and sts. Linkage map is shown in centimorgans. Marker names and positions are documented on the chromosome schematic along the *x*-axis. Horizontal lines indicate suggestive and stringent genome-wide thresholds.

heritability estimates, but are more susceptible to environmental effects. We examine the module structure controlling cortical-folding traits and assess the interplay between numerous biological domains: development, genetics, morphology, and neural connectivity. This helps to characterize the evolutionary constraints imposed on the system, dramatically affecting the potential for future cortical alteration. We observe high morphological integration between phenotype and genotype, which would readily allow for adaptive alteration of the cortex as a whole. We also theoretically test tension-based models for cortical development, finding support for their predictions over competing models. Finally, we ran genome-wide linkage mapping tests for the 10 metric features, identifying QTL regions that contain the genes affecting variation in gyrification and parse out the genetic architecture for this complex phenotype. QTL peaks identified include stretches that contain genes that have been previously implicated in brain development and function, and we additionally discover novel areas that have not previously been shown to be associated with cortical topology phenotypes in primates. Brain folding is a significant and unique trait with a complex genetic architecture, involving polygeny, pleiotropy, and numerous genes of varying effect.

This interdisciplinary study characterizes gyrification's underlying genetic makeup and elucidates the biological underpinnings contributing to structural and, ultimately, functional differences in the cerebral cortex between primate species. Our findings provide a foundation for further examination of the molecular basis for evolutionary changes in primate brain folding. Although this work was done in the baboon, the results are more widely applicable and can be used to inform human genetics and neuroscience, as there are numerous neurological disorders characterized by abnormal cortical gyrification.

Acknowledgments

We thank Henry Kennedy (Stem-Cell and Brain Research Institute) for allowing us access to his and his collaborators' extensive connectivity data set before its publication and Charles Hildebolt and Kirk Smith for guidance with the radiology and imaging aspects of the study. Revisions and suggestions from Bruce Carlson, Glenn Conroy, Charles Roseman, Alan Templeton, and David Van Essen were pivotal to this project's completion. This work was supported by the National Science Foundation (BCS-1260844, BCS-0725068). Nonhuman primate resources used in this study were supported by the Southwest National Primate Research Center grant from the National Institutes of Health (P51 OD011133, formerly P51 RR013986). The authors declare that they have no competing interests.

Literature Cited

Abdul-Hay, S., and T. Sahara, 2012 Identification of BACE2 as an avid β-amyloid-degrading protease. Mol. Neurodegener. 7: 46.

Alberts, S. C., and J. Altmann, 2001 Immigration and hybridization patterns of yellow and anubis baboons in and around Amboseli, Kenya. Am. J. Primatol. 53: 139–154.

Almasy, L., and J. Blangero, 1998 Multipoint quantitative-trait linkage analysis in general pedigrees. Am. J. Hum. Genet. 62: 1198–1211.

Balzeau, A., R. L. Holloway, and D. Grimaud-Hervé, 2012 Variations and asymmetries in regional brain surface in the genus Homo. J. Hum. Evol. 62: 696–706.

Barton, R., 2006 Primate brain evolution: integrating comparative, neurophysiological, and ethological data. Evol. Anthropol. 15: 224–236.

Bayly, P. V., R. J. Okamoto, G. Xu, Y. Shi, and L. A. Taber, 2013 A cortical folding model incorporating stress-dependent growth explains gyral wavelengths and stress patterns in the developing brain. Phys. Biol. 10: 016005.

Bellugi, U., L. Lichtenberger, W. Jones, Z. Lai, and M. St. George, 2000 I. The neurocognitive profile of Williams Syndrome: a complex pattern of strengths and weaknesses. J. Cogn. Neurosci. 12(Suppl. 1): 7–29.

Bhoiwala, D., I. Koleilat, and J. Qian, 2013 Overexpression of RCAN1 isoform 4 in mouse neurons leads to a moderate behavioral impairment. Neurol. Res. 35: 79–89.

Bruner, E., 2003 Fossil traces of the human thought: paleoneurology and the evolution of the genus Homo. Rev. Antropol. 81: 29–56.

Bruner, E., 2004 Geometric morphometrics and paleoneurology: brain shape evolution in the genus Homo. J. Hum. Evol. 47: 279–303.

Bruner, E., 2007 Cranial shape and size variation in human evolution: structural and functional perspectives. Childs Nerv. Syst. 23: 1357–1365.

Bruner, E., 2008 *Comparing endocranial form and shape differences in modern humans and Neandertal: a geometric approach*. PaleoAnthropology, 1: 93–106.

Carlson, K. J., D. Stout, T. Jashashvili, D. J. de Ruiter, P. Tafforeau *et al.*, 2011 The endocast of MH1, Australopithecus sediba. Science 333: 1402–1407.

Charpentier, M. J. E., M. C. Fontaine, E. Cherel, J. P. Renoult, T. Jenkins *et al.*, 2012 Genetic structure in a dynamic baboon hybrid zone corroborates behavioural observations in a hybrid population. Mol. Ecol. 21: 715–731.

Chatterjee, A., and S. Dutta, 2013 Potential contribution of SIM2 and ETS2 functional polymorphisms in Down syndrome associated malignancies. BMC Med. Genet. 14: 12.

Chen, H., T. Zhang, L. Guo, K. Li, X. Yu *et al.*, 2013 Coevolution of gyral folding and structural connection patterns in primate brains. Cereb. Cortex 23: 1208–1217.

Chen, Z. J., Y. He, P. Rosa-Neto, J. Germann, and A. C. Evans, 2008 Revealing modular architecture of human brain structural networks by using cortical thickness from MRI. Cereb. Cortex 18: 2374–2381.

Cheverud, J. M., 1984 Quantitative genetics and developmental constraints on evolution by selection. J. Theor. Biol. 110: 155–171.

Cheverud, J. M., 1995 Morphological integration in the saddleback tamarin (Saguinus fuscicollis) cranium. Am. Nat. 145: 63–89.

Cheverud, J. M., 1996 Developmental integration and the evolution of pleiotropy. Integr. Comp. Biol. 36: 44–50.

Cheverud, J. M., D. Falk, M. Vannier, L. Konigsberg, R. C. Helmkamp *et al.*, 1990 Heritability of brain size and surface features in Rhesus macaques (Macaca mulatta). J. Hered. 81: 51–57.

Cookson, W., L. Liang, G. Abecasis, M. Moffatt, and M. Lathrop, 2009 Mapping complex disease traits with global gene expression. Nat. Rev. Genet. 10: 184–194.

Cox, L. A., M. C. Mahaney, J. L. Vandeberg, and J. Rogers, 2006 A second-generation genetic linkage map of the baboon (Papio hamadryas) genome. Genomics 88: 274–281.

Dray, S., and A. Dufour, 2007 The ade4 package: implementing the duality diagram for ecologists. J. Stat. Softw. 22: 1–20.

Duggirala, R., J. T. Williams, S. Williams-Blangero, and J. Blangero, 1997 A variance component approach to dichotomous trait linkage analysis using a threshold model. Genet. Epidemiol. 14: 987–992.
Enlow, D., 1990 *Facial Growth*. WB Saunders Company, Philadelphia.
Van Essen, D., 1997 A tension-based theory of morphogenesis and compact wiring in the central nervous system. Nature 385: 313–318.
Falk, D., 1986 Endocranial casts and their significance for primate brain evolution, pp. 477–490 in *Comparative Primate Biology Vol. 1: Systematics, Evolution, and Anatomy,* edited by D. R. Swindler and J. Erwin. Liss, New York.
Falk, D., 1987 Hominid paleoneurology. Annu. Rev. Anthropol. 16: 13–28.
Falk, D., 2014 Interpreting sulci on hominin endocasts: old hypotheses and new findings. Front. Hum. Neurosci. 8: 134.
Feingold, E., P. O. Brown, and D. Siegmund, 1993 Gaussian models for genetic linkage analysis using complete high-resolution maps of identity by descent. Am. J. Hum. Genet. 53: 234–251.
Gibson, G., and G. P. Wagner, 2000 Canalization in evolutionary genetics: A stabilizing theory? BioEssays 22: 372–380.
Gómez-Robles, A., W. D. Hopkins, and C. C. Sherwood, 2014 Modular structure facilitates mosaic evolution of the brain in chimpanzees and humans. Nat. Commun. 5: 4469.
Groves, C. P., 2001 *Primate Taxonomy.* Smithsonian Institution Press, Washington, D.C.
Hartigan J. A., 1975 *Clustering algorithms*. Wiley, New York, NY.
Hartigan J. A., 1985 Statistical theory in clustering. J. Classif. 2: 63–76.
Hartigan, J., and M. Wong, 1979 Algorithm AS 136: a k-means clustering algorithm. J. R. Stat. Soc. Ser. C. Appl. Stat. 28: 10–108.
Heidemann, S. R., and R. E. Buxbaum, 1990 Tension as a regulator and integrator of axonal growth. Cell Motil. Cytoskeleton 17: 6–10.
Heidemann, S. R., and R. E. Buxbaum, 1994 Mechanical tension as a regulator of axonal development. Neurotoxicology 15: 95–107.
Herculano-Houzel, S., B. Mota, P. Wong, and J. H. Kaas, 2010 Connectivity-driven white matter scaling and folding in primate cerebral cortex. Proc. Natl. Acad. Sci. USA 107: 19008–19013.
Hijazi, M., C. Fillat, J. Medina, and A. Velasco, 2013 Overexpression of DYRK1A inhibits choline acetyltransferase induction by oleic acid in cellular models of Down syndrome. Exp. Neurol. 239: 229–234.
Hilgetag, C. C., and H. Barbas, 2006 Role of mechanical factors in the morphology of the primate cerebral cortex. PLOS Comput. Biol. 2: e22.
Hirata, Y., and C. Zai, 2012 Association study of GRIK1 gene polymorphisms in schizophrenia: case–control and family-based studies. Hum. Psychopharmacol. Clin. Exp. 27: 345–351.
Holloway R., D. Broadfield, M. Yuan, 2004 *The Human Fossil Record: Brain Endocasts -The Paleoneurological Evidence,* edited by J. H. Schwartz and I. Tattersall. Wiley & Sons, New York.
Huang, H., R. Xue, J. Zhang, T. Ren, L. J. Richards *et al.*, 2009 Anatomical characterization of human fetal brain development with diffusion tensor magnetic resonance imaging. J. Neurosci. 29: 4263–4273.
Hutchison, D. W., and J. M. Cheverud, 1992 Fluctuating asymmetry in tamarin (Saguinus) cranial morphology: intra- and interspecific comparisons between taxa with varying levels of genetic heterozygosity. J. Hered. 86: 280–288.
Im, K., H. J. Jo, J.-F. Mangin, A. C. Evans, S. I. Kim *et al.*, 2010 Spatial distribution of deep sulcal landmarks and hemispherical asymmetry on the cortical surface. Cereb. Cortex 20: 602–611.
Jolly, C. J., 2001 A proper study for mankind : analogies from the Papionin monkeys and their implications for human evolution. Yearb. Phys. Anthropol. 44: 177–204.
Kaymaz, N., and J. van Os, 2009 Heritability of structural brain traits an endophenotype approach to deconstruct schizophrenia. Int. Rev. Neurobiol. 89: 85–130.
Klingenberg, C. P., 2008 Morphological integration and developmental modularity. Annu. Rev. Ecol. Evol. Syst. 39: 115–132.
Kobayashi, Y., T. Matsui, Y. Haizuka, N. Ogihara, N. Hirai *et al.*, 2014 Cerebral sulci and gyri observed on macaque endocasts, pp. 131–137 in *Dynamics of Learning in Neanderthals and Modern Humans*, Vol. 2, edited by T. Akazawa, N. Ogihara, H. Tanabe, and H. Terashima. Springer, New York.
Kochunov, P., D. C. Glahn, P. T. Fox, J. L. Lancaster, K. Saleem *et al.*, 2010 Genetics of primary cerebral gyrification: heritability of length, depth and area of primary sulci in an extended pedigree of Papio baboons. Neuroimage 53: 1126–1134.
Korenberg, J. R., X.-N. Chen, H. Hirota, Z. Lai, U. Bellugi *et al.*, 2000 VI. Genome structure and cognitive map of Williams syndrome. J. Cogn. Neurosci. 12: 89–107.
Krubitzer, L., 2009 In search of a unifying theory of complex brain evolution. Ann. N. Y. Acad. Sci. 1156: 44–67.
Lander, E. S., and L. Kruglyak, 1995 Genetic dissection of complex traits: guidelines for interpreting and reporting linkage results. Nat. Genet. 11: 241–247.
Lloyd S., 1982 Least squares quantization in PCM. IEEE Trans. Inf. Theory 28: 129–137.
Lu, J., G. Lian, and H. Zhou, 2012 OLIG2 over-expression impairs proliferation of human Down syndrome neural progenitors. Hum. Mol. Genet. 21: 2330–2340.
Mackay, T. F. C., 2001 Quantitative trait loci in Drosophila. Nat. Rev. Genet. 2: 11–20.
Mahaney, M. C., S. Williams-Blangero, J. Blangero, and M. M. Leland, 1993 Quantitative genetics of relative organ weight variation in captive baboons. Hum. Biol. 65: 991–1003.
Markov, N. T., and P. Misery, A. Falchier, C. Lamy, J. Vezoli, *et al.*, 2011 Weight consistency specifies regularities of macaque cortical networks. Cereb. Cortex 21: 1254–1272.
Markov, N. T., and M. M. Ercsey-Ravasz, A. R. Ribeiro Gomes, C. Lamy, L. Magrou *et al.*, 2014 A weighted and directed interareal connectivity matrix for macaque cerebral cortex. Cereb. Cortex 24: 17–36.
Martin, R. D., 1990 Primate origins and evolution: a phylogenetic reconstruction. Proc. Biol. Sci. 263: 689–696.
Meunier, D., R. Lambiotte, A. Fornito, K. D. Ersche, and E. T. Bullmore, 2009 Hierarchical modularity in human brain functional networks. Front. Neuroinform. 3: 37.
Meunier, D., R. Lambiotte, and E. T. Bullmore, 2010 Modular and hierarchically modular organization of brain networks. Front. Neurosci. 4: 200.
Moss, M. L., and R. W. Young, 1960 A functional approach to craniology. Am. J. Phys. Anthropol. 18: 281–292.
Mota, B., and S. Herculano-Houzel, 2012 How the cortex gets its folds: an inside-out, connectivity-driven model for the scaling of mammalian cortical folding. Front. Neuroanat. 6: 3.
Preuss, T. M., M. Cáceres, M. C. Oldham, and D. H. Geschwind, 2004 Human brain evolution: insights from microarrays. Nat. Rev. Genet. 5: 850–860.
R Core Team, 2012 *R: A Language and Environment for Statistical Computing*. R Foundation for Statistical Computing, Vienna, Austria. ISBN 3-900051-07-0, URL http://www.R-project.org/.
Rogers, J., M. C. Mahaney, S. M. Witte, S. Nair, and D. Newman, *et al.*, 2000 A genetic linkage map of the baboon (Papio hamadryas) genome based on human microsatellite polymorphisms. Genomics 67: 237–247.
Rogers, J., P. Kochunov, J. Lancaster, W. Shelledy, D. Glahn *et al.*, 2007 Heritability of brain volume, surface area and shape: an MRI study in an extended pedigree of baboons. Hum. Brain Mapp. 28: 576–583.

Rogers, J., P. Kochunov, K. Zilles, W. Shelledy, J. Lancaster *et al.*, 2010 On the genetic architecture of cortical folding and brain volume in primates. Neuroimage 53: 1103–1108.

Rosenberg, K., and W. Trevathan, 2002 Birth, obstetrics and human evolution. BJOG 109: 1199–1206.

Sawada, K., K. Fukunishi, M. Kashima, S. Saito, H. Sakata-Haga *et al.*, 2012 Fetal gyrification in cynomolgus monkeys: a concept of developmental stages of gyrification. Anat. Rec. (Hoboken) 295: 1065–1074.

Sporns, O., D. R. Chialvo, M. Kaiser, and C. C. Hilgetag, 2004 Organization, development and function of complex brain networks. Trends Cogn. Sci. 8: 418–425.

Stalling D., M. Westerhoff, and H. -C. Hege, 2005 Amira - A highly interactive system for visual data analysis, pp. 749–767 in *The Visualization Handbook,* edited by C. D. Hansen and C. R. Johnson. Elsevier, NY.

Stevenson, R. E., 2006 *Human Malformations and Related Anomalies*. Oxford University Press, Oxford.

Streitbürger, D., K. Arelin, J. Kratzsch, J. Thiery, J. Steiner *et al.*, 2012 Validating serum S100B and neuron-specific enolase as biomarkers for the human brain: a combined serum, gene expression and MRI study. PLoS ONE 7: e43284.

Sun, T., C. Patoine, A. Abu-Khalil, J. Visvader, and E. Sum *et al.*, 2005 Early asymmetry of gene transcription in embryonic human left and right cerebral cortex. Science 308: 1794–1798.

Toro, R., M. Perron, B. Pike, L. Richer, S. Veillette *et al.*, 2008 Brain size and folding of the human cerebral cortex. Cereb. Cortex 18: 2352–2357.

Ventura-Antunes, L., B. Mota, and S. Herculano-Houzel, 2013 Different scaling of white matter volume, cortical connectivity, and gyrification across rodent and primate brains. Front. Neuroanat. 7: 3.

Visscher, P. M., W. G. Hill, and N. R. Wray, 2008 Heritability in the genomics era: concepts and misconceptions. Nat. Rev. Genet. 9: 255–266.

Wagner, G. P., 1984 Coevolution of functionally constrained characters: prerequisites for adaptive versatility. Biosystems 17: 51–55.

Wagner, G. P., 1988 The influence of variation and of developmental constraints on the rate of multivariate phenotypic evolution. J. Evol. Biol. 1: 45–66.

Wagner, G. P., 1996 Homologues, natural kinds and the evolution of modularity. Integr. Comp. Biol. 36: 36–43.

Wagner, G., and L. Altenberg, 1996 Perspective: complex adaptations and the evolution of evolvability. Evolution (N. Y.) 50: 967–976.

Wagner, G. P., M. Pavlicev, and J. M. Cheverud, 2007 The road to modularity. Nat. Rev. Genet. 8: 921–931.

Williams, J. T., H. Begleiter, B. Porjesz, H. J. Edenberg, and T. Foroud et al., 1999 Joint multipoint linkage analysis of multivariate qualitative and quantitative traits. II. Alcoholism and event-related potentials. Am. J. Hum. Genet. 65: 1148–1160.

Winterer, G., and D. Goldman, 2003 Genetics of human prefrontal function. Brain Res. Brain Res. Rev. 43: 134–163.

Xu, G., P. V. Bayly, and L. A. Taber, 2009 Residual stress in the adult mouse brain. Biomech. Model. Mechanobiol. 8: 253–262.

Xu, G., A. K. Knutsen, K. Dikranian, C. D. Kroenke, P. V. Bayly *et al.*, 2010 Axons pull on the brain, but tension does not drive cortical folding. J. Biomech. Eng. 132: 071013.

Yushkevich, P. A., J. Piven, H. C. Hazlett, R. G. Smith, S. Ho *et al.*, 2006 User-guided 3D active contour segmentation of anatomical structures: significantly improved efficiency and reliability. Neuroimage 31: 1116–1128.

Zhou, C., L. Zemanová, G. Zamora, C. C. Hilgetag, and J. Kurths, 2006 Hierarchical organization unveiled by functional connectivity in complex brain networks. Phys. Rev. Lett. 97: 238103.

Zilles, K., E. Armstrong, K. H. Moser, A. Schleicher, and H. Stephan, 1989 Gyrification in the cerebral cortex of primates. Brain Behav. Evol. 34: 143–150.

Zilles, K., N. Palomero-Gallagher, and K. Amunts, 2013 Development of cortical folding during evolution and ontogeny. Trends Neurosci. 36: 275–284.

Zollikofer, C., and M. de León, 2005 *Virtual Reconstruction: A Primer in Computer-Assisted Paleontology and Biomedicine*. Wiley-Liss, New York.

Zollikofer, C. P. E., M. S. Ponce De León, and R. D. Martin, 1998 Computer-assisted paleoanthropology. Evol. Anthropol. Issues News Rev. 6: 41–54.

Communicating editor: L. E. B. Kruuk

GENETICS

Supporting Information
www.genetics.org/lookup/suppl/doi:10.1534/genetics.114.173443/-/DC1

Cortical Folding of the Primate Brain: An Interdisciplinary Examination of the Genetic Architecture, Modularity, and Evolvability of a Significant Neurological Trait in Pedigreed Baboons (Genus *Papio*)

Elizabeth G. Atkinson, Jeffrey Rogers, Michael C. Mahaney, Laura A. Cox, and James M. Cheverud

DOI: 10.1534/genetics.114.173443

File S1

Supporting Materials

Extended Description of Endocast Creation and Validation

The first third of skulls were scanned at the lower resolution threshold before switching to the higher resolution 0.6mm slices for the remainder of the skulls. We omitted 215 scans for use on the left hemisphere and 185 on the right. Exclusion from data collection was typically due to one or more of the following: the individual being a subadult (defined here as below 6 years of age) and therefore not confidently demonstrating adult gyrification patterns; the individual being older than our cutoff adult age of 30, after which brain shrinkage and intracranial remodeling can degrade endocast impressions; the individual being of a different species/subspecies than investigated here; lack of a clear endocast impression in the scan; or processing issues with digitization of scan files. In total, 770 CT scans were deemed fit to have data collected on the left hemisphere and 800 on the right. On the left hemisphere, 198 (26%) of measured endocasts were from male baboons and 572 (74%) from females. On the right, these numbers are 219 (27%) and 581 (73%), respectively. 3-D segmentation of CT images was allowed to run for 150 iterations until seeds had expanded against all surfaces of the endocranium. Sulci are then seen as depressions on the endocast, as they appear on brains. Spiral medical CT scans were used, as these provide more smooth segmentations than slice-wise CT scans.

Repeatability measures were calculated from the metric phenotypic data to validate the utility of CT-based endocasts for studies on cortical topography. Repeatability was calculated by comparing the difference between repeat measurements of the same sulcus. This also provides an estimate of the amount of measurement error present in the data. Individuals whose differences between repeated measurements deviated from the mean of the normal distribution for inter-measurement difference by greater than two standard deviations were removed from analysis as they were deemed to be unreliable. This resulted in removal of no more than 5 individuals per sulcus. Most cases of such unreliable endocasts were from extremely old individuals, as remodeling occurs on the endocranium during the course of animals' lives, diminishing the imprint of the brain on the interior of the skull. Other cases were due to damaged skulls or poor CT scan resolution. The average r^2 between double-measured metric traits was 0.93 for both the left and right hemispheres. These metric trait repeatability measures are very high and indicate the clarity of CT-based endocasts.

Measurements taken from CT scans were also compared to parallel landmark measurements collected from MR scans for 100 overlapping individuals in order to ensure that CT-based endocasts capture a representative impression of the brain (Kochunov *et al.* 2010a; b). The average MR-CT length difference was 6.61 mm for the left hemisphere and 7.72 mm for the right. The average correlation between landmarks taken on CT versus MR scans was 0.95 on the left and 0.96 on the right. The average correlation between the CT and MR measurements for all landmarks averaged over all individuals and sides was 0.95. CT measurements are thus typically shorter than the corresponding MR measurements, likely because of the tapering off of sulci towards their ends. This would create less of an imprint at tips of the sulci, shortening the impression on the virtual endocast mold. Since quantitative genetic tests are concerned with the variation around the mean rather than the mean value itself, a bias in absolute length between CT and MR scans would not affect quantitative genetic results, as traits measured from CT and MR are very tightly correlated. In other words, the variation is commensurate, even if the mean is slightly shifted. The extremely high CT-MR correlation shows that measurements collected on these CT based endocasts are a good representation of the brain's folding pattern. It further validates that CT-based virtual endocast creation is an appropriate manner in which to analyze sulcal impressions and does not distort the image in a way that would inhibit accurate interpretation of results. Only CT-based measurements were used in final analyses, so any difference between MR and CT values would not affect results.

Extended Explanation of Covariate Screening

CC was used as an estimate of overall brain volume in order to control for allometric scaling. CC data were collected for a different project using the same CT scans, and these data were kindly forwarded to us specifically for use here as a covariate (J. Joganic, personal communication). CC measurements were cube-rooted for comparison of units of equivalent dimensionality, as our sulcal lengths are one-dimensional. Sex was screened as, in general, male baboons are larger than females, causing them to have comparably larger

brains. The age of an individual was examined, as older individuals tend to be larger than younger ones, even among full adults. An additional consideration for age is that there is remodeling of the cranial vault over individuals' lifetime. In elderly individuals, the brain has retreated slightly from the skull, which could allow for diminishment of impressions of sulci on the interior of the skull. Animals over 30 were omitted from analysis for this reason. Only ~11% of our data was for animals over the age of 25 so old-age remodeling should not confound results, especially with consideration of age as a covariate. Age-squared takes into account the rate of change in sulcal length over the course of life. A significant result for the covariate of age x sex would imply that sulcal length and age have different slopes in the two sexes.

Files S2-S3

Available for download at
www.genetics.org/lookup/suppl/doi:10.1534/genetics.114.173443/-/DC1

File S2 Raw genotypes for all phenotyped animals that have accompanying genotypic data (840 total). The genotypes for every STR locus for animals are additionally publicly available via a searchable web interface at: http://baboon.txbiomedgenetics.org/Bab_Genotypes/PubGeno_Query.php.

File S3 The pedigree of the genotyped animals measured in this study. We used the matrices of multipoint IBD coefficients and whole genome linkage maps for analyses. Details related to the construction of the latter are published in: Cox LA, Mahaney MC, Vandeberg JL, Rogers J. A second-generation genetic linkage map of the baboon (Papio hamadryas) genome. Genomics. Sep;88(3):274-81.

SUPPORTING TABLES

Table S1 Raw phenotypic measurements for metric traits

ID	arsp	cs	iar	ips	lf	lu	ps	sar	spcd	sts
10009	7.79	54.36	27.31		45.96				18.86	61.56
10012	10.84	49.92	33.49	33.00	52.03	39.18	29.92	19.43	24.96	55.36
10016	6.48	48.42	27.10	34.91		36.94	28.82		11.46	
10039	7.12	49.82	34.04	39.81	51.54	37.93	32.24	14.61	22.77	59.08
10041	4.73	47.42	31.30	42.88				9.86	15.93	
10042	8.35	48.26	28.40	34.50	47.18	41.00	29.80	15.17	15.55	55.20
10044	5.81	45.86	30.83	36.21		31.70	30.17	10.89		
10046	9.16	48.68	32.14	30.35	46.76		26.11	22.31	6.02	52.28
10052	9.40	48.36	29.77	42.91	50.58	38.81	31.06	15.36	19.41	59.27
10054	9.36		29.15					10.18		50.24
10074	10.35	49.06	26.57	38.27	49.06	37.80		12.80		
10082	9.55	48.36	29.35	35.22	44.56	34.73	31.81	11.52	20.57	50.26
10090	9.46	48.62	38.69	32.13	42.19	41.95	32.09	22.70	19.56	52.13
10099	10.29	54.12	29.33	39.55	44.93	41.55	29.83	15.41		53.72
10120	8.17	47.17	28.06	42.07	46.37	38.25	28.58	11.16	21.23	55.87
10127	7.49	43.95	27.33		51.00		30.92	16.07	20.82	58.05
10128	10.83	47.60	29.61	39.72	52.90		30.95	13.84	15.44	59.76
10130	10.97	49.64	32.95	38.74	51.84	42.69	30.18	14.54	19.09	58.82
10153	10.17	47.93	27.96	41.40	50.15		28.90	12.55		60.00
10154	10.27	49.86	37.77	29.65	35.24	41.75	33.20	20.24	15.37	
10157	12.29	46.31	24.97	37.30	46.16	39.34	27.15	12.94	11.41	56.33
10160	4.16	46.93	29.50				31.65	15.68	22.30	
10161	10.54	52.14	33.93					10.25		
10164	12.60	48.02	30.35	36.46	48.79	39.04	35.32	16.28	24.08	57.63
10173	12.63	50.15	29.85						22.28	
10183	9.38	47.25	28.92	38.03		37.61	30.91	15.39		
10206	3.72	46.16	31.62				33.00	14.66	21.50	
10208	8.30	43.20	28.16	35.69	51.28	37.86	30.42	15.44	7.94	
10226	11.16	48.79	36.03					12.25		
10240	14.40	53.42	32.28						14.24	
10259	9.79	50.41	28.04				31.36	11.83	18.69	
10280	7.54	47.70	31.13					15.06		
10297	11.15	49.49	29.33	38.86	42.31	37.29	29.39	16.60	22.80	
10316	9.09	45.74	30.99	35.68	49.83	40.09	27.35	11.62	18.79	52.95

10347	3.77	47.92	31.42	37.17	46.99		31.36	15.59	23.84	61.73
10379	8.52	50.86		30.76					21.17	
10393	9.36	46.01	22.71					5.87		
10403	9.72	51.59	29.66	41.94	53.43	39.22	28.21	15.34	11.92	62.15
10418		47.69		34.48						
10429	11.27	47.59	26.64	39.35		42.72	29.15	9.53	10.09	
10430	9.89	49.47	32.69	37.34		40.43	32.32		22.12	
10433		51.08	46.73	30.77		46.30	28.39	27.99		
10492	6.17	48.08	30.77	40.49	53.77		29.17	17.83		
10504	8.52	47.16	30.36	36.94	44.31	34.27	29.27	13.13	19.16	
10509	7.74	46.61	23.07	34.36	45.91	34.24	31.35	14.18	12.59	41.76
10510	5.97	45.40	39.16	32.17			31.65	24.27	16.28	
10511	5.96	45.62	49.99	34.84	46.48	39.41	35.47	25.59	19.95	54.74
10520	13.36	49.09	33.44	42.27	55.95	46.88	34.39	14.27		60.88
10535	9.44	48.90	34.04				31.57	13.44		
10603				33.04	44.45	34.39				50.59
10611	4.54		37.67	30.35	50.35		30.20	22.49		53.21
10619	10.49	44.63	30.73	37.56	47.69	38.40	31.27	5.53		59.54
10728	2.54	47.40	33.19		49.63		30.18	13.84		
10729	6.02	47.39	28.47	42.88	53.77		28.13	18.33	17.61	
10734	4.62	50.04	31.11		52.46		30.71	12.65	18.04	55.91
10740	8.44	46.04	27.26	37.87	48.73	35.15	27.63	14.29		50.19
10741	8.69	47.20	31.60		55.09		32.63		21.41	68.62
10760	12.66	50.64	30.85	38.21	49.30	36.34	26.26		17.60	53.37
10841	5.32		32.05		49.34		30.84	6.96		55.20
10872	7.24	49.03	27.33	37.28	49.50		33.30	15.09	21.25	59.80
10875	9.17	51.08	35.09	31.57				18.36	21.32	17.11
10911	7.93	44.16	31.60		49.74		28.98	12.56	24.15	
10912	6.05	49.71	32.71				32.65	12.10	21.91	
10987		52.95	28.70	40.18		36.94	27.52	9.09		50.96
10988	7.06	45.30	30.74		46.83		30.26	12.39	21.61	56.51
11001	11.20	47.08	27.53	33.77	48.66	38.07	27.36	14.12	14.60	55.98
11009	10.17	45.94	28.53	39.39		42.48	32.01	13.67	21.35	
11015	8.05	54.22	27.01	39.41	53.86	38.84	29.25	16.76	13.58	58.04
11079		51.75	31.53	44.40	53.30		32.54	20.11		65.56
11163	8.97	44.92	28.32	38.74	49.89	37.55	27.90	11.26	25.70	54.20
11442			47.92							
11443	13.56	47.03					31.68	13.75		
11444	9.37	47.46	45.57	32.43	41.51	38.02	36.29	11.75	12.89	

11499	13.28	51.29	22.80	36.86	38.78	40.93	31.60	16.32	12.80	35.45
11581	8.67	46.05	23.42	34.87	49.30	36.78	28.64	14.00	15.58	46.38
11585	10.62	53.89	31.84	34.34	49.24	42.87	30.32	19.35	18.22	37.31
11600	2.96	47.25		36.01			30.63	16.48	17.66	
11617		47.79	43.55		40.22					48.94
11619	12.77		25.21				30.64	6.58	25.05	
11627	10.30	49.70	31.59	36.70			29.81		21.27	
11639	9.11	42.57	29.71	31.80			29.65	11.71		
11672		54.20								
11687	8.72	48.61	29.09		47.28		29.51	10.53		
11769	9.34	50.80	26.67	37.22	48.93	39.79	30.92	14.84	13.42	40.47
11886	9.86	46.41	29.02				27.65	11.74		
11992		47.84								
11997	2.72	47.38	29.21	36.76			28.91	10.51	21.23	
12157	8.29	42.01	28.46				26.82	10.97		
12162	6.65			24.76					12.60	
12175	4.29	43.82	30.51	35.93	49.39	37.59	28.05	15.21	19.14	60.21
12217	11.69	45.24	31.12	36.09	48.55	39.22	27.48	10.37		55.62
12226	9.80	48.46	35.12		47.96		30.81	20.88		51.53
12411	11.53	48.20	30.01	38.26	53.56	39.09	28.80	15.07	19.74	64.45
12417	5.54	45.78	29.81	34.58	45.69	41.77	29.39	14.91		
12457	11.93	51.87	30.68	38.22	43.30	41.19	30.20	15.93	16.93	49.13
12466	3.33	43.37	27.26		46.53		29.53	13.47	16.15	
12480	10.72		32.50				30.99	9.39	23.17	
12499		48.95	31.36		51.92		33.98			58.31
12513	7.75	46.46		36.09	53.79	36.25	24.21	8.46	7.84	
12639	9.32	46.43	27.10						20.91	
12720	9.73	47.25	22.30	39.92	41.01	36.51		12.36		50.19
12726	9.47		48.26							
12929	8.50		34.98					13.28		
13125	11.16		30.39						21.33	
13226		49.40	29.84		48.21		30.81	9.82		
13280	9.62	55.60	29.96							
13546	10.57		32.88						27.02	
13625	11.08	49.15	32.17		48.86		30.31	16.10		
13645	12.13	52.44	35.91		53.07			12.71		
13751	7.54		29.06					13.15		
13758	11.15	47.64	26.17	34.25			28.68	10.38	15.27	
13859	8.23		37.60	30.77	34.79		35.34	20.09		25.27

13947	9.53	48.89	30.64	38.21	51.26		31.31	21.74		
14039	4.11	51.51					34.16		22.15	
14044	6.15						27.40	10.43	9.21	40.44
14081	11.11		38.84					15.69		
14084	10.03			31.89						
14166	10.95	48.55	27.72	38.95	52.42			13.84		57.52
14167	7.45	41.52	31.38	33.92		34.88	34.01	16.98	15.41	
14204	10.27	47.70	22.44	33.49	39.27	36.46	27.00	10.02	10.31	40.82
14252			44.15		34.65					
14263		47.81	34.61							
14270	10.28	43.50	28.23	34.95	49.42		31.58	12.25	13.85	
14275	7.11		26.60	36.49		40.97	33.14	18.50	14.11	
14277	7.87		31.34					14.94		
14286	7.93	48.35	23.75	43.42	43.71	40.58	31.75	16.12	9.63	44.11
14322	3.58		31.47	31.05		31.29				
14324	1.75	46.56	23.35	39.50	43.81		29.52	19.17	16.86	51.81
14381	5.19	42.15	29.33	34.02		36.56	30.85	13.68	14.18	
14435		46.96	31.40				26.93	13.91		
14478	9.98	46.13	29.74					7.93	22.24	
14484	11.19	47.82	39.66	35.09		48.46	31.25	29.94		22.40
14499	8.90	45.19	26.51	33.78	49.88	40.43	29.99	13.01	8.64	
14508		51.03	26.05						15.91	
14665	8.86	41.99	24.33	36.00		31.19	23.64	14.51		
14676	6.42	49.33	30.41	36.45			28.98	15.98		
14695	9.01	49.37	27.59	36.49		37.70	28.72		18.42	
14696	5.22	43.12	30.78				29.97	13.26	15.69	
14710	3.29	49.79	41.88	31.38			33.72	23.72	11.76	
14744	9.46									
14754		55.35								
14796	8.19	42.98	21.71	32.83	41.44	33.20	24.92	12.91	11.78	
14859	4.86	47.26	26.75	32.43	50.57	35.40	29.87	11.97	14.82	60.62
14879	11.62	47.09	25.48		49.82			12.54		52.36
14883	8.61	46.49	24.86	28.82	45.73	39.88	29.00	12.44	14.46	50.14
14894		44.54	25.88		47.83					
14909	6.25	50.09	25.09	36.62	50.27	37.53	30.54	10.39	18.90	
14923	5.95	45.67	32.63	35.71	45.84		28.80	11.51	17.64	52.16
14931	4.11	46.06		35.63		32.38	27.37	12.42	16.69	
14955	8.07	48.71	31.55	37.38	48.34	37.66	30.13	18.99		48.57
14962	7.11									

14979	8.43	49.48	34.24				31.35	14.80	26.99	
14983	5.66	49.26		35.16	44.32		32.87	15.06	8.92	47.76
14993	11.49		32.26	37.56		35.05	28.04	20.95	24.42	26.46
14995	6.28	53.49	30.23	38.24	54.35	38.99	31.59	17.11	18.87	64.55
15140	8.01	40.59		37.39		35.18	32.49	13.53	14.80	
15150	7.22	45.28	30.83	37.38	49.30	37.06	32.07	15.23	19.69	61.21
15155		46.35	29.78	36.33			27.56			
15162	8.11	42.90	30.50	32.73		33.91		12.43	21.60	
15168	11.46		41.67	32.50		40.30		21.03		
15217	9.80	46.99	32.56						16.42	
15283	8.21	48.05	24.32	38.52	50.70	37.22	28.16	18.21	13.88	47.42
15293	7.70	45.34	24.33	35.42		33.64	28.37	14.68	12.46	
15423	7.48	46.02	28.58	35.57	49.71	41.41	26.81		13.81	
15444	4.67		22.58	30.35			28.21	13.20	10.50	
15464	11.04	48.71	26.81	38.63		37.73	30.52	13.39	17.08	
15506	9.93	44.02	31.03	36.08		37.10	28.32	16.30		
15527	9.34	53.42	35.89	37.19	56.76	43.72	31.19	16.20	15.77	56.19
15539	9.70		22.00					19.76	11.07	
15579	6.16						29.18	18.07		
15584	9.80	50.30	32.14	30.33	54.99		28.27	16.29	15.92	58.62
15588	6.88	51.07	33.12	40.72	49.67	35.87	31.05	19.05	18.92	
15634	9.10	50.59	33.09						18.48	
15639	7.48	50.81	24.62	38.10	43.57		30.44	15.28	18.94	
15654	8.40	51.06	30.75	40.42	53.37	42.71	33.61	19.01	19.17	62.20
15656	7.97	47.97	31.95	42.29	53.84	39.73	30.90	21.83	20.00	
15828	8.91	44.17	30.02	35.41	57.78	35.28	31.12	16.81	17.22	64.70
15843	9.76	46.44	29.15	34.07	48.32	34.30	32.12	10.02	23.24	51.11
15858	5.06	48.48	31.33	37.59	48.24	38.87	32.44	16.33	17.64	57.43
15885	2.06	46.19	28.14	33.35	50.10	35.98	34.17	17.32	15.41	54.66
15938	6.61	46.56	32.81		47.12		29.57	14.24		49.54
15973	8.63		33.20				30.12	13.56		
15976	8.46	52.22	30.27	37.59			26.70	14.39	15.01	
15988	10.37	48.19	29.03	39.33			29.96		21.37	
16073		47.38								
16102	8.71	50.00	30.68	36.72	48.27	36.65	32.72	12.83		54.28
16115	5.81		19.76	32.35	39.82	33.74	25.13	17.05	12.94	
16118	7.20		30.90				32.41	12.52	24.21	
16231	7.54	45.31	30.05		45.78		29.73	10.80		
16330	9.91		34.86	36.63		40.38	32.82	15.94	16.74	

16368	5.39	48.38	30.64	37.08			31.76		12.40	
16386	7.17	44.71	32.94	34.21	47.68		33.17	11.51	22.42	53.47
16495	4.61		32.12				31.05	11.79	12.05	
16576	9.86	49.44	30.07	35.19	56.64	34.89	33.06	14.48	16.29	67.40
16725	9.15	48.76	33.53	35.21				17.35		
16742	8.10	45.74	26.71	37.17			28.93	12.38	19.42	
16852		43.49							12.36	
17031	8.47	51.65	27.03	40.12	44.93	36.42	27.29	11.40	8.45	37.54
17111	8.11	47.48	28.07	37.83		35.25	28.42	16.70	14.73	
17214	11.52	43.60	22.35	39.71	43.24	37.96	27.62	13.59	14.64	
17230	6.11	47.62	32.27	33.62	49.24	37.78	31.68	14.05	13.48	60.78
17243	5.70		21.87				28.52	15.27		
17331	8.23						33.23			
17355	10.07	49.69	25.68	41.78	49.39	43.12	32.51	14.83	10.25	
17810	5.55	46.46	28.24	32.78		35.56	29.60	15.67	18.20	
17966	5.27	46.54	28.87				26.48	17.01	21.88	
18341	15.00	48.67	28.33	37.59		37.78	32.47	13.99	17.69	
18391	8.57	48.92	28.40	38.15		36.04	30.76	12.33	12.08	
18531	10.38	48.71	35.98					14.02		
18729	6.66	40.06	30.05	33.49	48.48		29.09	14.71	15.85	57.27
18737	5.68	51.24	33.40	41.95	47.60		34.75	18.40	19.39	62.08
18742	2.64	51.99	32.22				34.03	17.97	15.81	
18744	3.44	51.51	32.77	40.38	49.33		31.40	17.76	16.16	
1B0831	6.94	50.53		38.48	54.76	38.01				55.83
1X0351	6.88	47.88	31.10	37.21	45.27	41.07	29.42	13.57	19.83	
1X0681	7.32	48.39	28.59	35.42			24.62		17.29	
1X0684	3.01	46.78	27.84	37.56	50.66	42.09	26.34	18.60	12.09	57.91
1X0842	5.79	47.11	30.47	41.04		40.55	26.71			
1X0864					50.80					55.11
1X0937	9.30	43.77	25.71	32.71	47.72	35.73	25.64	16.23	20.14	50.95
1X0976	5.99	54.29	24.29	39.50			30.98	18.69		
1X1032	8.52	49.07	29.12	41.12	49.75	41.07	29.90	16.14	22.06	55.84
1X1146	4.47	45.78	30.56		53.76		30.22	13.41		
1X1166	10.29	46.16	30.01	32.30	52.25			28.44	14.40	37.86
1X1177	2.20	51.46	25.96	38.28		39.39				
1X1181	9.85	48.31	29.31	38.41	49.21	42.54	32.86	17.38	18.97	59.23
1X1224							32.38			
1X1237		44.34	33.23				29.35	16.68		
1X1257	9.13	46.25	29.52		58.40		30.27	13.90	19.82	

1X1374	11.25	50.41	31.23	40.20	52.85	45.97	28.43	14.71	17.49	63.97
1X1404	8.45		35.14				29.28	14.01		
1X1441	10.37	47.61	33.88	31.80		39.89		10.21		54.39
1X1447	10.13	49.22	31.13	38.17		43.07	30.78	16.57	18.88	
1X1557	9.35	48.13	28.35	39.46	49.61	40.15	31.50	15.31	19.87	58.31
1X1577	8.32	47.31	33.95	34.24	51.96	35.89		14.79	18.82	68.51
1X1656	7.54	45.91	32.74	37.47	52.46	37.98		9.08	21.45	58.63
1X1687	7.86	49.23	26.19	37.44	48.77	39.65	26.83	12.71	22.58	61.71
1X1734			31.56					14.15	15.88	
1X1763	10.11	45.12	29.70	38.20	55.26	37.36	30.28	16.36	15.47	59.85
1X1786	11.21	49.78	28.45	35.54	47.56	41.02	26.49	15.99	13.95	55.62
1X1864	10.28	49.42	29.92	34.20	48.37	38.45		11.27	18.90	55.90
1X1956	3.51		29.17				28.94		18.37	
1X1957	5.07	46.52	35.36	37.44	50.52	39.96	31.76	12.81	13.10	55.28
1X1958	11.02	47.00	27.99	37.55	46.77	42.43	29.90	19.28	24.88	53.40
1X1962		49.49	38.89	32.06	37.85	38.97	38.27			
1X2000	12.22		46.65	30.02		47.81				19.05
1X2033	9.82	49.43	28.09	41.02	55.70	36.31			19.22	54.18
1X2063	9.56	47.27	33.09				29.36			
1X2081	5.86	47.64	27.48	37.87	50.69	37.35	26.90	12.07	18.24	57.53
1X2092	9.87	55.17	37.01	43.66				14.95	19.34	
1X2100	5.05	49.00	27.89	37.19		36.67	30.19	10.95	16.38	
1X2117	7.45	43.84	28.37	32.53	43.56	38.26		10.37		
1X2124								18.58		
1X2172	8.35	44.72	31.78					13.36		
1X2176	7.83		46.16	38.43					14.14	
1X2199	12.11	45.45	29.20	39.90	48.66	40.24	26.63	13.00		57.10
1X2231	13.00	49.93	31.77	36.81		37.34	29.19	14.02		52.84
1X2269	7.32	50.01		38.08	50.47	37.11				50.70
1X2315	8.79	49.98	30.63	38.92	49.74	42.73	28.53	15.14	25.78	58.89
1X2360	7.78	41.84	26.01	37.05	46.90	40.82	28.29	13.93	18.24	51.24
1X2361	10.28	48.38	30.97	35.51	57.30	34.47	32.14	11.91	15.24	64.31
1X2365	2.89	48.14	29.11	36.46		41.07	27.58	12.66		
1X2379	8.67	39.80	28.90	36.42	45.90	36.67	27.77			52.08
1X2384	9.78	44.32	31.19	30.78	43.10	32.55	27.61	10.52	15.51	46.63
1X2490	5.32		30.25	28.73	49.33			29.21	16.53	34.40
1X2495	9.88	50.87	32.27	34.05	49.70	39.14	27.22			54.56
1X2509	2.48	48.89	41.73	31.57	34.64		34.72	17.90	15.80	
1X2511	10.84	49.30	30.26					11.82	21.46	58.36

1X2538							26.52	12.12		
1X2572	12.94	47.81	37.67					24.11	22.13	15.05
1X2574			29.64		50.07		26.80		15.45	56.24
1X2576	12.54	54.03	27.76	41.49			25.74	19.18	22.83	
1X2589	6.98		32.14	29.34			29.45	23.00	16.41	
1X2594	9.87	51.27	40.20	29.99			28.83	20.75	21.84	15.30
1X2624	10.03	46.61	27.73	38.76	50.43		32.80	14.23	21.22	55.02
1X2644	9.91	46.09	32.26	40.49	48.73	44.74		9.56		56.26
1X2684	5.04	47.11	34.00		48.05		33.50	17.36		53.36
1X2686	8.55	49.15	31.07	36.32	48.52	44.42	31.35	15.28	18.06	58.07
1X2697	8.55			28.12				30.32	13.31	
1X2699	6.84	50.70	34.04	40.48	44.14	48.73	31.45	15.08	21.01	52.51
1X2713	6.53	49.49	29.01			42.02	32.07			
1X2716	6.21	51.61	26.30				28.19	14.51	20.86	
1X2717	10.41	51.78	40.91						12.16	
1X2796	8.99	46.85	31.53	37.84	51.08	40.18		14.28		
1X2798	9.19	47.83	31.18	33.54	52.44	44.19	28.37	15.84		59.99
1X2813	8.16	45.55	31.12	36.00	46.16	39.45	29.57	14.57	20.01	54.35
1X2816	12.66	49.49	33.05	39.61	47.80		28.52		28.81	
1X2822	7.84	44.58	30.33	39.49	54.92		26.59	17.66	16.44	
1X2825	10.03	48.55	27.78	34.47		38.25	27.18	9.59		
1X2884		52.93			53.48				16.44	
1X2996	7.46	49.28	29.76	35.43	48.28	35.59	30.48	13.46	15.85	
1X3027	7.02	50.09	27.10				28.40	20.34	16.73	
1X3052	7.54		32.91	40.63			31.53	15.36	23.13	
1X3103	7.47	46.01	30.17		50.64		27.08	17.12	18.93	55.42
1X3104	9.49	53.23	31.44				29.61	15.24		
1X3144	7.79	48.37	34.71					16.59	16.81	
1X3162		55.89							21.56	
1X3195	8.23	46.68	32.73	38.60	53.93		33.39	16.21	18.93	59.51
1X3208	8.27	47.48	30.51					11.74	16.21	
1X3255	7.66	46.58	31.12				26.98	12.09		
1X3291	4.35	41.58	28.47				30.24	13.48		
1X3310	9.82	46.89	30.01	39.83		46.78	33.44	16.03	16.95	
1X3312	6.33	47.73	39.63	34.80	51.77	40.84		23.10	15.18	59.36
1X3337	3.91	49.19	30.28	39.18	48.45	39.90	29.73	16.67	18.97	59.33
1X3351	9.66	45.91	25.67		47.16		25.16	13.03	18.81	
1X3428	9.44	52.37	30.72	35.48	55.54	39.56	31.98	14.55		63.16
1X3432	7.65	46.56	31.58	40.00	50.11	38.83	25.63	9.96	14.92	56.28

1X3439	6.79		30.39	35.48	49.04	34.35		19.86		54.63
1X3445	8.03	46.85	38.13	32.14	43.83	44.45	30.31	22.59	16.69	37.55
1X3475	6.25	46.92	26.40	38.27	49.00	33.50	26.80	16.80	12.74	58.07
1X3521	7.45	44.48	37.50	30.71	41.91	39.58	32.60	23.56	9.23	49.69
1X3548		42.55								
1X3564	12.30	46.22	31.45	36.89	53.19	39.55	27.58		20.08	
1X3567	8.24	47.66	26.74	38.16	49.20	40.15		15.58		51.03
1X3581	1.78		34.82				29.70			
1X3582	6.04		38.64	34.33	49.31	39.08				52.52
1X3592	9.32		37.10	32.75	40.95	37.50		28.39	10.25	16.01
1X3593	6.49	47.42	30.72	46.13	49.66	36.71	31.04	12.99	21.09	56.00
1X3594	9.73	47.98	34.98	38.72	54.37	43.97	30.44	17.04		60.70
1X3597	5.40	51.36	30.73	38.88	50.01	42.14	29.22	15.49	21.09	
1X3637		49.04	26.77	43.02		35.70	29.03	14.47	21.36	
1X3641	2.31	57.38	47.21	29.23				28.66	12.72	
1X3648	9.45	51.66	31.63	40.77	49.58	43.60	29.99	11.96	27.73	52.31
1X3649	10.99	52.65		35.81		38.76	27.24	13.93	11.69	
1X3653	11.16	45.91	30.18				25.95	13.98	23.14	
1X3655	5.49	45.70	29.28				30.40	14.88	20.96	
1X3666	7.10	53.20	32.62		42.65			15.69	13.93	
1X3671	7.16	43.98	24.21	34.21		34.05	30.97	12.62	11.61	
1X3679	9.00	48.65	30.07		52.11		32.44	15.89	22.86	63.16
1X3687	3.98	47.56	29.75		49.90		30.63	13.76		
1X3690	9.01	46.41	27.41	35.78	44.69	37.35	26.52	12.27	21.22	
1X3696	8.40	47.26	38.76	36.89	47.47		37.21	14.84	13.29	60.13
1X3701	7.83	45.22	26.00	32.95	45.55	34.65			19.07	46.26
1X3705	7.86	47.86	27.34		44.46			14.06	18.14	
1X3731	8.46	49.82	33.03	30.15			29.69	20.38	13.29	
1X3739	6.67		34.08				33.44	15.44		
1X3740	5.02	46.50	29.25	36.72	45.57		30.04	14.37	16.82	54.40
1X3749		44.95						16.19		
1X3757	6.61	50.68	33.71						23.18	
1X3764	10.31	50.91	28.91	41.69	52.10		30.51	14.33	17.68	61.44
1X3765	6.04	46.98	31.95	36.71	47.12	38.10	30.80	19.40	16.40	54.88
1X3767	6.08	48.06	37.79	40.26			30.70	12.42	21.72	
1X3771	6.77	45.35	26.78	36.70	50.18	40.36	30.45	11.12	14.87	57.26
1X3774	5.29	46.17	23.76	40.16			28.93	12.57	10.81	44.02
1X3782	11.82	51.86	28.02	41.38	50.61	35.70	32.67		20.62	55.36
1X3783	11.05	50.05	30.28	36.17	47.72	41.84	29.43	17.78	25.14	56.56

1X3786	10.39	51.64								
1X3790	5.42	49.52	34.06	37.18	49.81	43.73	30.75	14.85		61.40
1X3796	5.91		33.52					14.25		
1X3805		47.57							18.79	
1X3808	8.81	47.76	31.09	38.98	50.08	36.59	31.42	13.94		57.58
1X3809	9.85	45.08	33.02	39.68	54.64	38.77		13.38	22.14	61.35
1X3810	11.50	47.72	31.81				31.68	6.58	24.75	
1X3812	8.09	45.97	28.99	38.36			29.52	15.24	21.52	
1X3814	10.16	51.07	39.31	31.58					13.18	
1X3817	6.50		30.11					19.00	15.31	
1X3818	5.84	47.84			51.05			17.22	18.49	54.13
1X3823	8.33	49.29	31.51	40.64	51.42	41.38	33.26	16.19	19.28	65.16
1X3828	9.91	50.35	27.63	39.90	49.52	39.45	27.99		22.99	58.07
1X3830	5.52	47.66	32.08	38.37	52.96	43.94	33.40	12.96	12.07	61.02
1X3834	7.79	49.67	29.11	34.96			31.65	16.80	17.08	
1X3836	9.03	46.26	29.59	36.57	47.99	38.84	28.07	12.40	17.71	
1X3837	7.98	45.63	33.41	35.01	50.97	42.06	30.19		21.89	55.29
1X3846	8.17	46.13	29.50		46.61				22.41	
1X3848	10.52	48.84	41.00	33.35				22.54	19.14	21.92
1X3849	9.18	44.69	26.09	35.18	46.02	37.22	28.32	12.36	12.82	
1X3861	5.61		33.21	33.59	49.66			21.10	17.35	34.17
1X3864	6.41	47.51	44.47	35.61	52.85				18.74	15.63
1X3867	9.39	47.55								
1X3870	13.26	54.35		40.92	51.23	41.87	31.64	13.27	15.30	
1X3882	10.11	48.25	30.07		48.55		28.04	15.98		58.34
1X3883	6.89	42.42	38.68	31.55			29.33	18.32	12.28	
1X3886	8.97	45.51	38.06	28.57	43.38		35.01	17.16	10.99	
1X3887	10.36	49.13	26.42	36.65	51.09	37.04		14.32		
1X3895	9.61	49.00	38.61	31.50		38.36	33.82	20.95	17.31	33.01
1X3899	8.46	47.94	28.54	39.05	46.80	35.89	26.58	13.05	21.27	50.82
1X3914	9.70	47.64							15.62	
1X3926	1.92		31.94				29.92	14.77	16.11	
1X3928	9.18	49.09	41.65	31.74				17.10	16.35	
1X3929	5.59		32.29	34.79	39.06	40.45	29.84	21.49		
1X3930	7.42	43.61	28.72				31.34			
1X3939	6.46	47.80	33.02	33.38	45.66	36.17	26.28	11.90	14.57	51.33
1X3947	8.35	46.68	32.91	27.21			31.08	23.67	19.50	
1X3948	6.75	46.53	31.65		42.14		29.16	13.14		
1X3952	11.68	55.05								

1X3956	7.16	50.53	41.45	34.57	43.47		34.14	21.67	14.99	36.11
1X3960	13.25	50.55	50.73	27.63	39.95			31.19	12.26	
1X3997	7.57	48.16	33.35				32.21		20.68	60.99
1X4006	9.10	51.05	27.73	40.19	48.72	36.61	27.99	15.36	16.78	55.41
1X4009							28.99	7.20	17.32	
1X4013	9.33	54.22	35.94					12.48		
1X4019	8.70	45.40	24.49	38.39	47.06	38.97	28.11	15.14	10.04	52.31
1X4031	6.68		35.14	28.08			28.87	22.45	12.39	
1X4032	3.63		25.44	36.95	41.82		26.34	15.22	17.76	54.23
1X4033	6.14	46.65	27.99				29.51		16.52	
1X4035	12.19	45.40	40.64	37.74	43.78	40.33		13.06		52.43
1X4038	8.34		25.72	37.97	51.91	41.64		11.32		60.88
1X4039	11.06	44.92	28.47	35.81		39.28	27.80	13.70	20.84	
1X4041	9.95	46.83	31.13	40.78	51.78	37.91	30.93	16.21	24.57	61.89
1X4045		49.96		36.17	47.93	37.72	27.99		14.43	54.61
1X4051	9.98	47.09	31.11	38.06	48.25	36.45	28.53	14.00	19.07	54.39
1X4052	8.81	45.61	23.18	35.33	51.88	35.13	28.93	12.92	10.21	44.80
1X4056		46.28	32.25	33.67			28.58	16.53	14.92	
1X4058	6.47	48.46	41.81	34.22	50.09	43.95	31.04	29.51	15.91	52.42
1X4064	7.72		27.90		49.43				24.72	53.95
1X4069	9.64	45.30	29.17	36.71	45.96	36.83	30.49	13.35		
1X4074	8.20	48.84	26.64	34.33	52.94	41.75	29.93	15.12	21.20	60.32
1X4077		50.51		36.31	57.39	35.99	29.70	12.16		60.90
1X4082	7.66	46.22	26.91	37.97		40.58	29.96	17.50	16.29	
1X4090	9.00	48.17	31.08	39.29	50.14	42.16	31.28	16.64	16.98	48.60
1X4091	4.20		27.69		48.32		28.11	16.88	24.57	54.16
1X4092	8.02	50.02	28.98	37.76	48.17	39.94	28.81	17.56	15.57	56.74
1X4096	10.21									
1X4108	7.41	47.88	30.24		52.24		30.74	17.47	21.19	57.23
1X4112	6.54	55.64	29.07	32.12	40.73	41.96	33.15		15.36	49.19
1X4121	6.77	44.15	33.26	37.60	50.48	40.64	32.98	13.77		
1X4143	6.76	50.77	33.46		48.43		32.00	14.16	16.02	
1X4146	7.66	42.24	27.50	34.38	43.20	35.30	27.07	15.46	15.14	50.00
1X4149	7.55	47.26	30.16	32.35	46.20	37.62	26.80	13.92		50.66
1X4154	11.23	49.15	35.02		50.78			16.86	24.85	59.96
1X4161	8.28	46.94	34.60	25.80	35.25		28.35	20.45	15.71	18.26
1X4162	8.37	45.16	31.80	36.14	44.97	34.60	29.36	12.38	20.53	52.48
1X4165	10.69	49.49	27.97	35.96	50.13	36.67	31.01	16.73	19.41	57.89
1X4166	11.21	50.75	28.04		57.69		28.11	16.41	16.74	61.82

1X4169	10.02	50.18	32.43		50.77		30.56	13.05		
1X4178	10.36	40.86	30.41	36.87	47.64	35.11	30.96	18.04	18.94	52.66
1X4179	9.31	52.86	45.85				31.94		17.92	
1X4183							28.99			
1X4184	4.91	44.81	29.71	33.92	49.71	39.89	28.66	11.89	17.40	57.83
1X4186	6.99	48.97	32.42				31.11	11.29	23.26	
1X4194	8.42	49.44	24.20	35.45		40.57	26.69	14.77	16.83	51.80
1X4195	4.93	47.52	27.41		49.28		30.24	14.89		
1X4209	12.96	49.90		29.43						
1X4213	7.42	50.51	32.66	40.41	48.30	43.34	30.58	14.88	25.06	55.79
1X4217	4.34	42.96	27.56	34.09		37.12	27.25		18.02	42.80
1X4218	6.98	46.87	26.39		48.66			6.96		
1X4221	8.26		26.77					15.15		
1X4222	4.40	42.91	31.91	36.11			30.48	14.43	23.14	
1X4230	5.85	45.46	31.36	38.81	55.04	40.36		15.71	18.16	59.25
1X4236	7.38	52.20	39.42	27.06	36.67	45.10		28.68	10.56	
1X4239	8.95	44.89	27.58		48.59				20.47	
1X4241	7.70	46.58	34.35	30.72				22.29	14.19	18.77
1X4243	2.02	52.84	29.53				30.81	12.95	21.44	
1X4246	8.90		44.69	32.78						
1X4248	7.67	44.77	25.17	35.53	41.75	36.66	26.18	11.69	9.59	43.49
1X4251	10.93	48.01	28.59	39.06	49.38	39.21	31.10	12.44	22.90	56.25
1X4257	7.61	48.36	33.40	36.25	51.29	41.22	28.73	14.55	20.09	53.38
1X4265	11.25	47.99	38.07	31.11	43.14	39.97	36.67	10.86	11.44	54.31
1X4268	11.51	42.37	41.99	31.82	47.91	37.65		12.32		47.58
1X4272	9.37	48.58	26.70	37.64	46.05	39.24	27.88	13.83	14.58	50.28
1X4273	3.83	42.46	25.53							
1X4276		43.61	31.25		47.89		27.44		23.44	
1X4277		48.07	44.29					16.96		
1X4278	9.45		40.72	31.24	52.41		31.59	20.78	15.33	52.14
1X4284	9.41		45.98	30.41						
1X4286	8.59	50.61		40.20		46.66		14.00	17.27	
1X4290	3.39	49.89	30.76		49.34	43.89	27.47			59.22
1X4294	11.07	42.23	34.45	37.02	50.51	37.00	30.51	15.48	19.22	
1X4303	6.94		40.85	30.21			31.25	12.39	10.27	
1X4308	4.11	45.65	31.02	34.81				13.78	12.87	
1X4314	2.29	48.07	30.59				29.36	12.61		
1X4315	7.24		34.45	39.07				12.25		
1X4323	5.16	49.25	30.57	42.86	54.22			17.11	14.77	56.84

1X4326	9.76	45.80	45.85	30.20				13.06	14.22	
1X4329	6.77	51.47	41.15	33.34	43.71		33.61	22.86	11.44	54.00
1X4331		47.86						16.72	19.71	
1X4519	3.03	47.88	31.78	38.18			29.99	13.11	18.52	
1X4558	10.87	55.30	26.79	36.94		40.54	28.98	12.96	21.97	
1X4593	7.57	49.17	27.09		46.30		26.85	12.96	12.74	56.24
1X4609	10.55	50.74	28.87	37.35	48.64	34.51	31.73	12.73	25.32	
1X4611	7.87	43.97	27.04	34.21	45.31		27.84	12.22	13.99	
1X4615	8.79		28.13	38.47	47.41	35.73	29.47	18.56	15.69	63.43
1X4627	11.06		51.95	32.80					14.33	
1X4631	8.14	49.82	38.97	25.31			31.60	13.71		24.48
1X4634		45.73		36.04						
1X4637	6.50	47.34	30.89							
1X4638	5.15	49.95	28.06	38.93	50.57	42.51	33.53	13.59	14.22	53.94
1X4642	6.43	45.21	30.12	37.75	48.75	39.09	31.91	13.55	14.32	60.48
1X4645	8.33	50.93	40.73	31.23			31.75	20.18	20.30	36.71
1X4647	9.69	50.61	38.17					13.79		
1X4648	6.18	49.30								
1X4687	8.47	47.74	27.03	37.40		37.11	28.85	12.76	18.29	
1X4710	1.78	46.62	26.87	38.49	50.32	37.59	25.08			56.83
1X4714	13.65	47.02	30.49	40.12				18.47		
1X4721	12.05	50.17	29.99	44.90		41.88	29.95			
1X4736	6.87	52.49	30.80		53.70	41.35	27.87	11.24	13.91	44.64
1X4739	10.34	43.97	23.03	34.34	42.66	38.80	28.19	8.85	10.98	42.39
1X4741	4.52	46.60	32.84							
1X4746	1.87	49.29	44.14	27.78			32.27	29.01	12.54	
1X4748	10.14		33.36							
1X4749	8.36	47.48	28.46	37.49	49.89	40.82	29.89	12.85	17.45	52.93
1X4752	6.93	48.39	41.93	33.73		49.42	32.13	16.52	15.02	
1X4760		52.46		40.86					18.70	
1X4765	9.89	47.88	29.26	39.24	49.59	44.05	30.13	7.93	25.29	57.86
1X4767	10.80	49.19	31.31	37.86	47.48	40.92	31.73	12.00		52.63
1X4771	11.61	50.10	39.40	31.85	52.69		28.65	18.29		51.55
1X4777	7.61		29.97						17.36	53.44
1X4779	7.66	47.14	22.06	30.38	40.43	43.32			9.35	
1X4782			27.98				33.47			
1X4792	8.24	45.71	26.75	39.73		34.51	30.49		15.48	
1X4808	10.68		45.89							
1X4820	7.08	48.21	31.67	37.85	47.86	41.01	29.69	13.12	16.57	54.15

1X4837	12.03	50.90	31.31	37.02	47.28	40.27	27.83	15.90	16.05	59.97
1X4842	9.59	49.93	35.63						15.82	
1X4850	8.16	48.56	32.46	38.08	53.95	45.31	31.55	11.23	21.40	58.93
1X4851	6.26	49.18	28.13	37.16	45.80		31.49	12.25	10.87	43.84
1X4859	12.35	47.47	30.79							17.59
1X4866	8.94	49.97	27.45	35.33	43.75	37.38	28.68	9.54	16.88	45.48
2X0236	10.21	46.50	33.22	37.50	51.59	39.85	30.43	13.77	23.60	56.22
2X0252	9.21	50.21	23.38	39.07	47.20	43.91	23.84	14.03	19.79	52.43
2X0253	7.73	46.80							18.70	
2X0331	7.15	42.90	21.71	31.90	40.60	30.04	26.86	9.06	10.27	
6215	8.70	43.68	31.79	34.68	45.99	36.83	28.89	13.65		53.99
6218	11.15	47.81	31.03	39.33	51.56		32.90	13.93		53.72
6222	7.03	44.80	31.49	32.58	50.61	40.06	28.74	11.32	13.34	58.54
6265	6.72	46.53	26.99							
6280	4.87	46.48	28.65				30.25	14.20	12.76	
6284	7.93	50.24	32.77	40.41	45.37	36.92	30.82	14.89	17.60	53.46
6290	5.33	47.68	27.90	34.03	43.47	39.64	26.49	14.49	11.99	49.43
6301	7.67		30.63				24.38			
6311	8.06	44.08	28.69	35.77	53.44	39.58	29.97	15.24	18.00	58.95
6312	10.66	45.28	32.00	33.00		37.46		19.52		
6315	6.34	45.06	25.71	33.38	40.80	42.78	28.09	10.43	11.20	51.84
6321		47.80								
6334	10.13	50.18		39.33		38.31	28.54	14.23	13.47	
6335	11.19	48.28	28.19	34.31	48.20	36.49	30.89	19.40	19.52	56.01
6342	7.30		22.31	37.31	41.44	35.00	25.39	10.01		39.97
6354	7.35	45.15	39.35	30.30	41.83	42.12		13.62	18.34	57.34
6355	10.02		25.57	41.70	47.44		28.35	12.49	20.07	61.54
6415	5.52	50.96	29.40	43.49		37.03	31.84	15.85	16.58	
6450	4.19	47.51	34.73	39.68		43.87	31.17	16.35	18.24	
6451	10.12		32.12		52.15					
6521	8.86	50.56	28.75					6.58	14.95	
6528	12.47	47.68	30.27		49.23		29.36	13.30	23.75	53.93
6531	7.50	49.47	24.36		40.61	32.31	26.36	12.16	11.65	
6585	8.79	51.77	29.30	42.50	49.03	41.89	30.65		19.69	
6600	10.15	53.14	30.63	43.14	51.61	41.20	34.08	9.73	10.86	
6622	4.13	46.96	33.79		49.33		35.51	17.86	21.22	60.89
6626	9.06		29.30	36.39		34.67	26.35	17.53		
6649	7.77	46.98		41.43	54.43		26.36	15.15		58.68
6668	9.22	41.39	25.59	35.46	46.10	34.77	29.36	12.38	5.18	

6690	9.22	49.95	37.10	26.71	46.53	40.99	31.00	21.09	11.79	30.85
6701	8.42	44.02	30.87		51.32		30.30		20.66	
6714	9.22	46.87	27.55	36.07		37.20	30.38	10.42		
6716	11.62	52.84	29.37				28.94	12.75		
6717	8.02	46.55	24.11	33.79	41.41	37.71	28.53	16.51	21.40	61.02
6725	7.52	50.95	33.48		52.32			16.47	13.92	56.38
6732	6.49	48.74	30.79				31.61		14.86	
6734	5.93	45.01	31.53	37.23			31.66	20.78	17.76	
6738	5.81	46.32	26.62	36.50	42.03	41.14	29.60	19.36	19.77	
6740	6.81	44.76	27.30	36.56	47.07	34.23	25.75	13.35	20.50	51.73
6746	9.08		32.86					16.63		
6753	4.25	48.91	32.34	36.76	50.99	42.22	30.11		15.30	58.63
6756	6.89	47.22	23.68	34.12	42.13		26.92	12.68	9.48	38.14
6776		48.03							14.62	
6793	7.88	48.75	31.01		48.70		33.67	15.82	17.21	57.16
6800	5.88	49.10	28.66	33.99	47.16	34.25	32.26	13.30	12.04	54.93
6802	5.62	46.55	26.36	33.90	43.93	38.29	29.02	19.84	14.08	56.08
6812			29.36				29.04			
6819	8.67	49.54	41.64	30.49			30.18	30.92	20.63	19.50
6821	9.60	47.29	31.32	34.37			29.89	8.53		
6838	6.77	47.14	27.87	41.92		36.23	28.61	14.87		50.44
6840	7.28	47.48	27.00	35.41		35.58	28.31	12.58	12.04	
6860	10.05	45.91	30.24		52.31		27.83	12.72	22.83	54.59
6903	4.61	53.28	35.01		52.14	45.54	35.16	16.64	20.41	65.30
6933	7.68		30.15				28.38	15.94		
6937	8.45	48.87	27.18	39.36	46.31	38.98	29.85	10.35		54.08
6948	12.31	47.74	28.45	40.79	41.01		30.65	14.21	23.45	
6949	7.51	42.85	32.71		44.81		30.33	19.27		
6955	7.97	49.69	32.29	40.74	49.60		30.90	15.12	22.42	60.26
6956	8.23	48.43	30.42	37.94	44.52	47.30	31.95	15.87	14.68	51.73
6965	13.56		36.57				34.04	13.75		
6968	6.38		36.85	27.80	38.67		33.07	26.51		
6971	5.42	50.72	31.08	36.27	48.13	33.79	30.74	15.62	14.56	
6977	7.60		43.13	38.33	37.80			24.44	15.25	21.05
6995	8.79	46.21	24.16	34.17	51.74	42.77	30.23	11.05	12.04	
6997	11.07	48.77	40.39	29.73	35.02		33.77		13.80	
7017	6.04	48.22	32.04	33.94	46.40	36.11	33.15	13.66	13.56	54.45
7031			47.45							
7052	11.81	51.61	33.32	39.86	57.74	46.41			21.34	59.23

7096	9.20		41.28	33.28	42.87	43.50	39.03	23.95	18.42	36.52
7122	5.98	46.25	26.43		48.23	38.82	29.36	14.27	16.98	57.41
7126	8.25	48.01	27.87	40.93	49.84			12.48	24.46	55.64
7137	8.74	49.49	21.04	34.67	44.22	33.32	26.61		11.06	
7158	10.31	49.97	32.11				34.12	12.22	12.01	
7190	8.94	52.30	34.70				34.20	10.75	19.40	
7196	7.95	47.68	27.55	39.14	49.88	39.02	27.57	15.47	11.54	57.76
7199	9.70		30.58	37.00		36.44			22.41	
7210	1.88	49.41	30.11	33.61	52.59	32.05	29.95	15.17		63.99
7211	1.86	46.48	26.67	35.55		37.70	30.53	13.54	17.47	59.90
7223	8.96	52.85	30.99		56.49				13.63	
7229	7.50	52.05	24.85	40.71		39.62	32.63	16.69	18.13	
7248	2.82		28.24			38.95	29.97	11.54		47.23
7267	9.48	45.86	20.30	30.50	43.72	35.71	26.85	11.85	13.28	50.01
7294	6.59	46.54	30.18	40.30	51.43	40.19	27.55		15.86	58.12
7329	10.32	47.12	28.96	41.42	53.37	41.41	30.82		23.51	60.15
7335	7.83	47.20	30.15			32.31	29.96	17.95	15.74	
7366	10.63	46.47	25.32	35.19	51.96		27.99	10.97	20.74	
7368	5.72		29.18				28.69	14.45		
7380	8.66	48.45	31.26	40.51	51.19	42.51	32.11	16.28	23.71	
7394	7.88	49.64	32.35	39.97	48.76	40.80	33.09	11.72		58.62
7398	10.13	51.76	32.74	37.17	49.32	37.87	30.47	9.68	16.71	58.02
7430	6.92	46.09	26.99	37.47		38.87	30.63	13.85	15.23	
7438	6.49	47.04	32.73			40.33	33.63	15.01	21.26	
7445	10.73	51.97	31.38	42.35	56.99	40.83	26.21	17.20	25.34	66.54
7446	8.75	47.91	26.34	35.31	48.76	39.21	25.86	14.57	17.84	55.29
7455	6.03		48.16	28.99				32.07		
7472	6.90		27.45					8.43		
7478	11.98	46.47	26.83	34.97	50.20	37.05	28.54	15.66		58.22
7500	11.63		30.37	40.74	52.16		29.09	12.99	21.31	
7538	5.22	49.48	34.47	36.63	48.70	37.23				54.58
7561	9.57	45.60	40.13	36.33	47.08	39.35	30.94	18.91	15.00	41.49
7606	6.63	49.80	30.24	33.69	47.52	36.08	29.88	13.34	10.71	58.58
7621				28.89				27.22		
7633	8.68	47.94	27.60	38.01	49.53	37.18	31.02	17.41	16.40	58.56
7634	7.18		25.56					13.41	18.90	
7635	10.25	52.21	40.50	30.19	48.63	48.79	29.52	20.26	14.14	34.56
7644	11.04	44.71	27.81	32.74	46.20	35.84	28.06	9.88	14.02	53.87
7645	4.43	46.43	28.00	36.04	50.18	40.23	30.28	14.23	14.14	55.39

7663	10.78	48.50	32.37	34.41	47.46	35.51			19.36	53.21
7675	12.61	51.07	30.18	41.60	49.78		28.51	16.32	13.92	60.04
7701	12.06	47.63	31.44	34.75	51.20		32.78	13.31	10.83	60.13
7716	8.32	46.65	26.82		49.02		30.67	13.93	22.76	54.83
7720	9.61	44.34	25.14	33.60	46.83	35.55	28.35			
7735	10.03	51.64	28.99	40.66		41.92	31.85	13.09	18.48	
7764	8.97	46.90	29.98	36.89		41.88	28.32	11.06	17.65	
7777	10.60	54.19	28.94	41.35	53.69	40.25	29.86	13.81	14.69	65.60
7784	9.44	44.09	28.24	33.50	53.46	39.76	28.33	10.35	16.77	
7808		44.56	28.81		51.22		28.18	20.19		
7823	8.03	45.45	42.22	33.62			30.12	32.24	13.53	
7844		53.10								
7850	7.00	44.72	25.39	34.78			28.55	14.32		
7855			26.43							
7862	10.30	47.77	28.47	39.48	47.86	39.55	30.60	9.62	15.16	54.86
7872	9.06	50.17	30.47	39.30	49.60	35.48	32.53	6.94	16.97	57.07
7882	11.11	43.04	30.77		43.79				15.42	40.96
7920	9.32	43.08	29.12	36.72	46.56	37.38	28.13	14.08	15.49	
7944	9.38		30.67					8.88		
7963	8.15	47.61	22.06	37.87	45.79		29.99	22.56	18.66	45.16
8001	9.22		29.71						17.39	
8008	8.80	54.39							20.99	
8010	9.14	50.48	30.84		56.51		32.96	15.51	18.26	57.97
8024	10.30	48.02	27.22	38.47	50.69		27.51	6.17	17.66	56.40
8027	6.76	47.28	30.47							
8034	8.01	45.74	29.68				32.73	9.98	26.10	
8046	9.70	46.71	28.06	39.47	48.37	36.87	28.81	17.25	16.47	58.12
8058	7.33	45.26	29.77	37.19	49.09	41.71	32.05	12.59	20.45	54.97
8062	9.03	47.34	35.12	37.63		37.60	26.69	14.35		
8070		53.30								
8088	5.35	48.14	30.19		47.12		26.76	12.13	19.72	
8091	9.15		30.51					16.62		
8092	8.05	48.07	28.61	35.92	45.31	37.57	28.72	10.14	11.49	56.40
8094	7.34	45.13	25.26	37.37	40.90	40.74	28.47	13.68	17.79	40.04
8116	7.99	48.93	31.77		49.65		32.41	15.81		
8120	6.77	48.83	27.31	38.44	49.29	37.61	28.27	13.75	22.22	58.94
8129	7.30	41.72	38.67	32.12	42.16	40.38	29.15	28.87	13.70	37.62
8134	6.51	53.72	31.14	37.23	51.65	41.13	33.11	17.02	18.07	60.00
8170	9.10	51.42		36.64		43.64	28.22	13.75	17.06	

8183	4.69	46.69	30.60		48.89		33.02	16.94	19.56	59.44
8206	3.72	45.48	26.72	36.99	47.96	41.85	28.00	11.79	15.28	57.77
8212	3.84	48.73	29.02						21.44	
8221	10.24	50.06	27.88	40.75			28.91	14.30	20.53	
8246	7.01	48.06	28.26	35.21	49.53	35.82	29.67	12.73	14.88	55.51
8250	9.08	46.86	27.69	36.18	48.78	41.33	26.80	14.94	17.37	54.88
8251			34.16	37.10				33.77		
8274	9.12	45.70	26.63	32.58	44.07	40.74	28.80	15.01	9.83	54.95
8282	8.66		29.45				30.19	18.04	21.85	
8288			36.78				25.23			
8291	4.90	50.76	32.28	40.41	49.16	40.43	32.76	16.96	18.92	
8292	8.24	48.19	35.45		47.38			16.59		48.82
8296	7.45	43.66	39.78	32.44	49.53		32.57	20.08	13.36	35.72
8299	1.80	46.74	25.72	36.86		38.87	30.52	13.43	19.34	
8302		48.82		42.04	53.90	39.47			18.16	62.10
8307	10.34	46.73	27.54	35.92	49.21	36.34	29.03		14.44	55.90
8313	5.37	44.73	38.10	30.05	41.78		28.71	21.32	12.05	52.52
8322	7.15	48.12	26.14	36.86	51.00	45.18	26.83	15.47	18.04	62.78
8329		48.10							17.51	
8344	8.60	53.59	26.53						13.96	
8369	4.17		34.71					24.21		22.19
8395	4.27	46.58	33.27	34.12	52.04	43.13	31.09	14.33	15.23	
8427	10.04		30.69					14.08	18.08	
8465	9.98	53.00	28.84	37.31	52.40			15.70	18.55	63.34
8469	8.63		32.19	37.29				19.88	23.41	
8477	8.58		32.32							
8478	9.91			31.73				28.24		19.58
8499	3.38	49.77	29.18				29.57	12.36		
8510	8.26	43.02	28.66	33.76	42.70	39.08	28.76	9.92	14.51	
8512	11.45	45.24	29.01	37.67	54.40	38.98	29.39	7.77		61.66
8517	6.88	53.75	29.94				29.96			
8518		42.40	25.45					11.07		
8538	7.86	48.18	34.29	37.12	52.58	41.33	31.96	15.00		60.24
8574	8.59	45.84	25.45	36.88	42.79	40.05	27.09	14.65	13.58	52.16
8576	4.99	49.12	36.73		59.95		33.05	16.11	7.22	
8596	7.35	45.92	40.96	33.33			31.85	15.48	10.34	
8600	9.64	46.06	28.71	42.97		42.77	35.21	12.99	21.84	
8601	8.16	52.13	26.46					18.22	16.05	
8615	6.47	56.27	26.57				30.09		16.20	

8623	8.05	53.43		39.10	48.26	37.63	27.35		7.29	46.28
8635	8.64	46.01	42.24							16.77
8638	8.85	49.25	30.36		48.10		30.79	15.79	20.11	51.96
8644	5.84	47.93	27.81	36.80						
8667	6.95	43.28	30.63	37.16	47.04	36.90	30.92	14.60		54.77
8690	6.87	44.76	25.45	37.05	46.72	38.08	25.93	15.16	10.96	36.70
8698	9.71	50.90	29.37	39.43	52.12		30.88	11.73		55.69
8700	9.98	47.62	34.06	30.74			32.89	18.42	6.37	
8765	7.00	44.99	31.62	35.93	55.94	38.16	29.77	17.65	17.75	63.42
8767	9.92	45.87	44.46	31.29					13.59	17.38
8778	8.21	46.99	28.81	34.40	47.00	35.24	29.35	14.66	23.85	53.93
8780	9.72	48.65	30.91					15.13		
8786	11.63	49.02	28.21	33.22	46.69		31.22	18.79	24.17	52.15
8797	11.65	46.40	26.00	32.70	43.78		28.65	5.43		50.89
8807	6.93	51.39	23.30	43.14	44.77		28.07	17.25	11.69	44.66
8817	8.40	52.10	26.10		50.46		28.41	16.23	25.71	56.84
8820	8.79	53.45	33.00				33.46	11.92		
8822	8.04	46.96	31.27	38.17	54.43	43.51	28.49	17.35	20.64	64.93
8826	7.48	44.90	30.07	34.13	44.24	35.98	28.91	11.99	18.67	56.78
8827	6.53	48.66	26.12	36.85		37.41	27.33		15.91	
8860	7.80	51.85	30.70							
8864	9.08	43.95	35.38	40.79			29.56	15.70		
8877	8.44	46.19	28.37		48.74		27.67	12.98	14.79	50.51
8893	8.43	46.88	24.37	35.89	44.17	37.52	30.20	17.71	16.03	
8895	8.46	45.34	25.92	35.44	44.91	35.62	29.65	13.40	13.81	
8905	8.67	47.29	29.12		45.89		31.32	14.68	21.80	
8906	11.06	52.17						12.64	21.70	
8919	7.55	41.59	34.82					11.42	19.91	15.24
8926	7.93	46.38	31.89	37.30	47.65	37.28	29.41		16.27	
8928	4.49	50.26	32.07				33.74	14.79	20.37	
8937	4.24	47.88	30.53	41.26						
8941	10.01	51.88	29.41	33.61			27.39	22.40	11.44	23.79
8962	6.23	45.89	41.21	32.19				29.32		
8973	10.43	46.82	28.55	38.36	47.70	37.74	28.18	17.08	25.79	52.34
8975			47.52							16.91
8979	6.00		29.82					12.16	13.07	
8980	2.56	52.10	25.08	34.01		37.42	29.64	14.66	9.74	
9014	3.94		30.59					19.00		
9020	13.27		47.56	31.39				30.76	12.05	

9021	7.19	49.82	30.69	41.08	46.46	40.24	32.26	15.57		51.52
9039	9.80	49.53	32.04	39.78	52.21	47.60	31.70	16.03		53.89
9040	7.09	46.65	30.88	39.54	48.54	39.76	29.57	11.09		59.74
9045	2.74	45.28	30.63	36.94	49.70	41.43	30.45	16.53	18.91	58.46
9089	15.19		29.88							
9090	10.14	53.80	28.62	42.81	56.05	34.95	31.43	14.86	20.49	62.66
9092	10.34	48.36	25.82	41.88	49.46	38.18	28.07	17.96		63.31
9094	8.23		33.42				26.68			
9097	11.22	57.76	32.65	41.52	56.99	42.43	28.93			66.38
9099	8.29	44.76	26.32	40.08	48.64	39.13	28.50	13.06	15.17	54.50
9124		50.67							19.91	
9128	7.43	46.13	30.92	35.97	49.94	40.48	31.16	12.27	15.69	
9129	7.13	47.17	28.86	36.22	46.32		26.61	10.92	17.84	
9156		46.59								
9166	10.50	49.76	29.00	37.23	48.28	34.71	31.11	16.24	18.65	52.57
9174	11.13	54.54	23.33	34.84	51.41	40.31	31.18	6.32	18.18	61.64
9178	9.08	47.51	30.28	35.38	50.42	39.55	32.44	11.71	15.50	53.38
9193	7.93	48.27	37.79	28.39				29.10	10.26	
9203	10.59	49.33	29.51		47.36		33.22	15.96	23.51	58.97
9205	3.17	47.88	28.18	34.78	48.98	36.89	29.30	15.67	19.36	55.60
9261	4.43	53.16	28.81						14.15	
9265	9.46	46.26	19.02	33.20	40.87	29.41	25.90	10.62	8.06	38.47
9278	6.58	46.66	25.44		43.85	38.28	30.37	14.04	12.21	41.51
9279	7.03	51.82	30.06		49.11		27.84	14.34		49.88
9282	7.68	52.10	27.68	41.19		38.80	31.62	11.80	21.19	
9285	8.33	48.76	33.11	38.35	54.61	45.62	29.94	14.37	19.06	65.40
9288	6.55	41.93	35.43	29.40	40.98	37.29	32.49	24.63	16.21	
9305	6.40	44.50	24.80	33.88	44.95		29.81	16.71	17.15	48.83
9316	11.88	43.51		31.64	50.66	39.17	29.01	11.34		54.73
9326	10.90		29.16				31.31		19.56	65.67
9338	9.59	52.45	32.27	40.29	55.24	42.92	36.02	13.50	16.04	57.91
9340	6.44	46.31		37.18	43.92	34.73	27.72	12.42	7.75	39.61
9344	2.57		37.19				31.67	17.76		
9347	8.99	46.92	30.64		56.38		28.23		23.16	59.43
9356	8.96	48.38	35.63	39.08		37.52	30.87		20.79	
9361	6.78	39.77	24.74	29.26	40.46	38.69	25.42	7.41	12.58	
9362	8.23	48.75	30.70	36.13		39.09	32.31	15.23		
9363	12.42	49.96	34.72	38.95	55.62	42.67	31.53	13.64	20.34	61.03
9385	8.06	51.44	32.48	36.51	48.77		34.30	12.40		53.89

9388	12.85		38.79		40.57		28.84			
9417	8.25	45.98	26.43	37.78	52.44	34.68	28.75	13.97	13.95	62.94
9427	7.77		27.37				30.74	13.66	15.20	
9467	3.70	46.64	31.14		47.97		31.95	12.10	15.21	56.24
9468	5.11	48.99	27.32		47.30		28.37	14.50		
9472	10.23		36.48					16.93	21.75	
9481	7.17	45.46	30.26	41.93	48.75	43.52	33.10	14.69	13.64	56.35
9486	10.82	52.55	31.50	42.69	51.15	37.79	32.18	15.16	18.35	60.91
9494	12.76	49.13	29.54	39.82	53.17	37.31	29.89	16.48	21.45	56.70
9495	8.40	52.34	28.84	37.06	49.38	40.37	32.25	11.98	13.07	60.99
9502	5.36	45.81	41.59	31.16				24.12	17.33	23.13
9514	11.11	50.12	32.51	33.15		38.83	33.08	14.21	15.37	59.86
9515	8.63	49.84	30.73	38.32	52.27	41.88	29.93	11.53	19.76	56.41
9545	6.63	52.76	28.69		48.79		31.02	15.22	12.46	51.71
9562	9.62		33.52	41.23	56.47	41.42	30.40	16.55	19.45	62.87
9569	6.09	45.33	24.11	37.60	46.15	38.71	27.75	13.99	9.15	43.72
9576	8.58	47.51	24.07	37.82	49.59	41.29	30.01	9.48	9.45	45.62
9581	8.82	48.06	31.15	32.42	46.26	37.10	28.62	11.53	17.19	50.57
9586	11.10	48.71	27.14	35.98	44.07	39.94	26.25	13.38	16.18	62.20
9592	11.50	56.03	32.12	42.95	58.18	45.18	32.97		17.60	68.61
9623	8.45	47.11	32.32		51.44		29.45		17.08	54.95
9625	8.17		27.18	36.56			30.44	10.71	10.14	
9632	10.74	48.02	29.36	35.89	49.14		30.67	7.09	14.30	53.27
9635	5.00	49.21	28.16	35.23	50.78		30.17	19.15	20.39	64.26
9641	9.13	45.24	39.47	33.30	52.20			21.84	18.32	52.58
9643	8.44		33.15							
9646	5.77	44.81	28.92	32.66	43.78	37.04	29.05	13.94	16.74	49.19
9656	8.95	44.42	32.80	38.40	54.52			16.20	20.89	
9666	9.32	51.60	31.32	37.81	47.59	41.44	29.05	11.06		56.43
9675		47.59					32.47	9.54		
9694	5.39	48.45	35.42	39.04	47.94	42.23	32.07	17.86	15.09	
9711	4.22	50.97	31.90		41.89		29.16	13.44	21.07	48.84
9714		47.42	28.84	32.92		35.81	33.71	13.88	18.64	
9716	7.94	43.57	39.18	32.17		37.98				
9722	7.52	48.66	23.70	32.32			29.62	11.78	17.33	
9740	8.71	47.47	31.12		48.24		28.82	12.03	22.11	
9743	9.13	47.06	26.14	34.84	46.72		26.53	17.88	16.94	58.11
9765	9.79	47.19	28.41	37.37	46.34	41.98		7.12	14.01	51.18
9771	13.37	45.55	26.88	35.51			31.08	12.96		

9774	8.55		46.61	29.81					9.62	
9789	8.86	48.94	41.36	32.64	42.17		34.05	18.03	14.90	57.99
9791	3.76	44.06	32.52	35.09	46.31		33.90	14.07	16.19	50.80
9805	4.55	46.09	27.47	35.80	51.38	41.14	29.10	16.18	20.30	
9808	2.60	44.38	33.74							
9841	3.13	44.12	27.31	31.90	41.73	36.35	27.58	15.15	15.83	
9855	3.18	47.68	28.93	35.09	43.50		28.87	17.09	15.42	52.62
9878	7.37	43.90	32.59	32.17	50.70	37.49	31.84	15.16	18.31	53.93
9892	6.42		31.10							
9903			24.70					11.05		
9907	7.63	44.25	30.47	31.04	42.18	37.77	30.32	11.75	17.80	
9914	9.15	47.49	19.69	32.52	42.40	36.54	26.02	10.51	10.15	39.29
9969	9.61	49.53	27.23	42.08	55.21		30.16	11.58	18.41	62.25
9976	7.91	46.64	27.79	35.54	47.54	38.52	27.29	10.41	14.92	

Table S2 Raw phenotype scores for non-metric traits

ID	Sex	Age	Larsp_yn	Lcs_forked	Lspcd_yn	Rarsp_yn	Rcs_forked	Rspcd_yn
UN001	M		1	0	0	1	1	0
7777	M	13.07	1	1	1	1	1	1
1X4045	F	19.35			1	0	0	0
1X1786	F	22.99	1	1	1	1		1
UN002	F		0	1	1	1	0	0
7446	M	13.69	1	1	1	1	1	1
1X2699	F	27.43	1	1	1		0	
1X1957	F	28.1				0	0	1
9099	M	11.55	1	1	1	1	0	1
1X3771	F	20.33	1		1	1	1	1
1X3026	M	21.63						
1X1687	F	22.9	1	1	1	1	1	1
8600	M	11.84	1	0	1	1	1	1
12639	M	12.18	1	0	1	1	0	1
8046	M	13.13	1	0	1	1	0	1
1X4038	F	19.19	1	1	1	1	1	1
1X3939	F	19.74	0	0	1	0	0	1
1X3475	M	20.66	1	1	0	0	0	1
7645	F	12.01	1	0	1	0	1	1
1X4217	F	18.61	0	1	1	0	0	1
8979	M	11.01	1					
1X4166	F	18.23	1	0	1	1	0	1
1X4749	F	16.07	1	1	1	1	1	0
6215	F	15.5	1	1	0	1	0	0
1X4710	F	15.9	0	1	1			
1X3740	F	19.34	0	0	1	1	1	
1X2081	F	22.38	1	1	1	0	1	1
1X1181	F	31.17	1	1	1	1	0	1
1X0681	F	31.03	1	1	1	1	0	1
1X3782	F	19.98						
1X2315	F	21.77	1	0	1	1	1	1
7329	M	14.08	1	1	1	1	1	1
1X4765	F	15.89	1	1	1	1	0	1
10403	M	9.13	1	0	1		1	1
1X2686	F	30.3	1	1	1	1	1	1
1X3200	F	21.07	1	1	1	1	1	1
1X0842	F	33.19					0	
1X4632	M	16.52						
1X2813	F	21.12	1	1	1	1	0	1
1X2644	F	27.6		1		1	0	1

9765	F	10.32	1	1	1	1	0	1
1X4519	F	21.97	0	0	1	0	0	1
1X4156	F	17.97	1	1	1	1	1	1
8681	F	12.12						
1X0976	M	23.8	1	1	1	0		1
1X1177	F	28.64		1		0	0	1
6450	M	14.96	0	1	1		1	1
10603	F	8.57						
1X4777	M	16.02			1	1		1
1X3310	M	18.21	1	0	1	1	0	1
1X2231	M	20.7		0		1		1
1X3337	F	22.96	0	0	1	0	1	1
1X2624	F	25.8	1	1	1	1	0	1
1X3808	F	18.82	1	1	1	1	1	1
1X3818	M	18.42	1	0	1	1	0	1
8576	M	10.55	0	1	1	1	0	1
1X2822	M	19.82				1	0	1
8395	F	10.64	1	0	1	0	1	1
7633	M	11.68	1	1	1	1	1	1
1X3930	F	17.92				1		
6415	M	13.41	0			0	0	1
1X4286	M	16.74	1	1	1	1	0	1
8058	F	10.02		0	1	1	1	1
1X4162	F	17.34	1	0	1	1	1	1
1X3758	M	18.79						
8229	M	11.04						
1X2576	M	20.53	1		1	1	1	1
1X2816	M	19.85	1	1	1	1	1	1
1X2884	F	20.36				1		1
8120	M	10.86	0	1	1	1	0	1
1X3823	F	18.9	1	1	1	1	1	1
9021	F	12.04	1	1	1	0	0	1
1X3701	F	18.68	1	0	1	1		1
1X3764	F	18.18	1	0	1	1		1
7478	F	12.12	1	0	1	1	1	1
9090	M	9.32	1	0	1	1	0	1
1X2360	F	20.25	1	0	1	1	0	1
1X4802	M	13.92	1	0	1	1	0	1
1X1447	M	21.06	1	0	1			
7126	F	12.68	1	1	1		0	1
1X4782	M	15.66						
1X3783	F	19.88	1	0	1	1	1	1
1X4767	F	16.2	1	0	1	1	0	1

8250	F	9.24	1	0	1	1	0	1
6649	F	11.7	1	1	1	1	0	
1X4184	F	15.8				0	0	1
1X4146	F	16.11	1	1	1	1	1	1
6284	F	12.9	1	1	1	1	1	1
1X0351	F	29.48	0	1	1	1	1	1
1X4051	F	17.05	1	0	1	1	1	1
1X3705	M	17.72	1	0	1	1	0	1
1X1257	M	22.04	1	1	1	1	1	1
1X0684	F	28.01	0	0	1	0	1	
1X2495	F	26.09		1		1	0	1
1X3805	F	17.79						
8282	F	9.68	1					
1X4064	F	16.95			1			
1X1958	F	25	1	0	1	1	1	1
1X4186	M	15.85	1	0	1	0	1	1
1X1224	F	28.01		0				
1X3997	M	16.15	1	0	1	0	1	1
1X3255	F	27.77	1	1		1	0	1
1X3162	M	22.87					1	1
1X4703	F	12.91						
8928	M	8.94	1		1	0	1	1
1X3899	M	16.51	1	0	1	1	1	1
1B0831	M	27.03				1	1	1
1X4842	M	13.23	1	1	1	1	1	
8638	F	10.25	1	1	1	1		1
1X1146	F	29.4	1	1	1	0	1	
1X3790	F	17.22	0	1	1	0	1	1
9279	F	11.99	1	1	0	1	1	1
1X3828	M	20.54		1	1	1	1	1
1X3195	F	22.1	1	0	1	1	0	1
1X3597	F	21.17	0	0	1	1	0	1
1X1374	F	25	1	1	1	1	1	1
1X3567	F	21.47	1	1	1	1	0	1
1X1032	F	27.99	1	0	1	1	0	1
1X0937	F	26.07	1	1	1	1	1	1
1X4090	F	19.66	0	1	1	1	0	1
1X2063	M	23.99				1	0	1
1X4820	F	16.39	0		1	1	1	1
1X2054	F	31.86						
1X4290	F	19.35						
9481	F	12.02	1	1	1	0	1	1
1X2365	F	23.18		1		0		

1X3809	M	20.68	1	0	1	1	0	1
1X3648	F	21.84	1	1	0	1	1	1
1X4091	F	19.73				0	1	1
1X3593	F	19.65	0	1	1	1	0	1
1X3679	F	20.87		1	1	1	0	1
1X3655	M	19.86	1	1	1	0	1	1
9347	M	10.27	1					
1X4810	M	16.67						
6451	M	16.24				1		
9740	F	11.09	1	0		1	0	1
1X2798	F	23.09	1	0	1	1	0	
8877	F	12.32	1	0	1	1	0	
7445	M	13.05	1		1	1	0	1
1X2891	M	27.98						1
1X1763	F	24.18	1	1	1	1		1
1X2172	F	29.17	1					
1X2511	F	27.6	1	0	1			
1X3887	M	20.42				1	0	
9344	F	9.91	0		1			
1X3837	M	20.57	0	1	1	1	0	1
1X4230	F	19.12	1	1	1	1	1	1
1X3291	F	22.13	0	0	1	0	1	
1X4019	F	20.37	1	0	1	1	1	
1X4331	M	19.09					0	1
1X0864	F	26.18						
1X3564	F	22.13	1	1	1	1	0	1
1X4634	M	17.92		1			0	
8066	M	13.7						
1X3822	M	20.95						
1X2379	F	23.37	0	0	1			
1X3902	F	20.7						
10316	F	10.3	1	0	0	1	0	1
1X2602	F	23.21						
1X1656	F	22.62	1	0	1		1	
1X3103	F	22.61	0	1	1	1	1	1
1X3432	F	22.24	0	0	1	1	0	0
8581	F	13.19						
1X2794	M	23.21						
8010	M	12.05	1	1	1	1	1	0
1X4748	M	17.19	1		1			
1X4041	F	18.22	1	0	1	1	0	1
6218	M	16.76	1	0	0	1	0	1
9045	F	12.73	0	0	1	0	0	1

1X1879	F	24.25						
1X1237	F	28.99	0	0				
1X1734	F	29.67				0		
6626	F	15.37	1					
8302	F	13.41	1	0		1		1
8973	F	12.69	1	0	1	1	1	1
1X2538	F	27.87						
1X2092	F	22.11	1		1	1	1	1
9039	F	12.33	1	0	0	1	0	0
8864	F	10.96	1	1	0	1	0	1
1X4294	F	19.35	1	0	1	1	0	1
10195	F	9.49						
1X2269	F	23.74		0		1	1	
1X4323	M	19.16	0	0	1	1	0	1
10729	M	8.97	0	0	1	0	0	0
9643	M	13.94				1	1	1
1X3867	M	21.1				1	0	1
1X3144	M	22.75	1	1	0	1	0	1
1X2033	M	20.92	1	1	1	1	0	1
9472	M	11.81				1		1
1X3594	F	19.85	1	0	0	1	1	0
1X3767	F	20.87	1	0	1	0	0	0
9878	F	10.97	1	0	1	0	0	1
1X2675	F	31.62						
1X4108	F	20.34	1	1	1	0	1	1
1X2490	F	27.93	0	0	0			
1X4853	M	17.21						
1X4268	F	19.67					0	
1X2199	F	24.29	1	1	1	1	1	1
6701	F	22.53	0	0	1			
1X4183	F	20.55						
1X2713	F	23.66		1		1	0	1
1X3327	F	22.82						
10760	F	10.09	1	1	1	1	1	
7199	F	15.52	1					1
1X2796	F	23.39	1	0		1	1	1
6860	F	16.25	1	0	1	1	1	1
1X3653	F	22.01	1	0	1	1	0	1
1X3697	M	22.18						
7937	M	14.5						
6965	M	15.32	1					
11446	M	25.35						
10226	M	11.21	1	0			1	1

1X3052	F	31.14	1		1	1		1
1X1956	F	33.7			1	0		
1X1404	F	31.69	1		1	1		
1X4154	M	20.11						
8000	F	14.62					1	
1X3707	F	22.17						
1X4326	M	19.15	1		1			
9502	F	12.37	1	0	1	0	1	1
6977	M	15.54	1					
1X4035	F	21.02	1				0	
1X3521	F	22.87	1	1	1	1	1	1
1X1166	F	26.61	1	1	1	1	1	1
1X3581	M	22.84	0					
1X4179	M	20.8	1	1	1			
18741	F	10.93						
1X3960	M	21.69	1	1	1			
1X3819	M	22.2						
1X4058	F	21.17	1	0	1	0	1	1
9641	M	12.71	1	1	1	1	0	1
1X4771	F	18.02	1	0	1	1	1	1
1X2509	F	28.98	0	0	1	0	0	1
1X1962	F	29.97		0	1	1	0	1
1X4209	M	20.82		0				
1X3431	M	23.11						
8635	F	14.06	1	1	1	1	0	1
8296	F	16.54	0	1	1	1	1	1
8129	F	16.56		1	1	1	1	1
1X3928	F	23.87	1	1	1	1	1	
6746	F	18.41	1	1	1			
10154	F	13.69	1	1	1	1	1	1
10090	F	14.01	1	1	1	1	1	1
10510	F	12.58	0	1		1	1	1
14435	F	6.91		1	1			
10433	F	13.27		1	1	1	1	1
7635	F	17.39	1	0	1	1	1	1
1X4631	F	19.98	1	1	0	1		1
8975	F	15.16	1			1	1	1
17812	F	18.79						
1X2000	F	26.19				1		1
8679	M	15.1	1					
10379	M	13.24	1	0	1	1		1
14187	F	6.37						
7895	F	16.53						

7882	F	15.9	1	1				
7031	M	18.04					1	
8251	M	16.59						
1X3956	F	22.72	1	0	1	1	1	1
8021	M	16.45						
1X4329	F	21.03	1	1	1	1	1	1
1X4284	M	21.72				1	1	
11585	F	11.09	1	1	1	1		1
8941	F	15.06	1	0	1	1		1
6690	F	17.88	0	1	1	1	1	1
14263	M	6.61	1	1	1			
1X4161	F	21.92	1	0	1	1	1	1
1X4647	M	20.53	1	1				
1X3445	F	24.34	1	1	1	1	1	1
9020	F	20.4				1	1	1
9193	F	14.65	1	1	0	1	1	1
1X4236	F	21.73	1	0	1	1		
1X4278	F	21.98	1	1	0	1	1	
1X2594	F	25.93	1	1	1	1	1	1
1X3548	F	27.28						
1X2176	F	30.48	1	1	1	1	1	1
11442	F	28.23						
11444	F	20.65	1		1	1	1	
1X3582	F	24.07	1	0	1	0	1	1
7621	F	16.74						
1X4031	F	23.27	0		1	1	0	
9906	M	13.25						
1X3952	F	22.02	1	1	1			
12162	F	9.88				1		
8767	F	15.23	1		1	1	0	1
1X2572	F	26.01	1		1	1	1	1
14252	F	6.16					1	
1X2589	F	26.05	0		1			
14266	M	6.99						
9288	F	14.24				0	1	1
1X3439	F	24.21	1	1	1	1		0
8597	F	15.13						
7866	F	16.38						
14322	F	6.79	1			1		
10012	F	13.59	1	1	1		1	
14081	M	6.39	1		1			
1X3420	M	24.46						
1X3883	F	23.16	0	0		1	1	

6997	F	17.33	1	1	0	1	1	
1X3814	F	23.86	1	0		1	1	
9789	F	14.28	1	0		1	1	
1X3886	F	24.47	0	1	0	1	1	0
1X3938	M	24.14				1	1	0
1X3312	F	25.38	0	1	1			
14993	F	6.27	1		1	1		
7842	M	16.05						
12929	M	9.66						
14484	F	7.34	1	1	1		1	1
10611	F	13.05	0		0	0	1	0
1X3696	F	25.38	0	0	1	1		0
9716	F	13.85	1	0	0	1	1	0
1X3864	M	24.34	0	1	1	1	1	1
1X2697	F	32.47				1		1
6354	F	19.78	0	1	1	1	1	1
1X2717	F	26.61	1	1		1	1	1
14373	F	6.21						
1X4418	M	22.38						
1X4022	M	22.39						
8962	M	16.38	0	1	1	1	1	0
12726	F	8.83				1	1	1
1X3848	F	24.9	1	0	1	1	1	1
1X4265	F	22.65	0	1	1	1	1	1
8062	F	16.25	1	1	0			
6968	M	19.09	0				0	
1X4627	M	21.23				1		0
15473	F	6.23						
14084	M	7.35				1	1	1
1X3739	F	24.88	1					
1X4686	F	20.87						
8070	M	17.57			1			
15168	F	6.83	1		0	1	1	0
1X4752	F	20.84	0	0	1		0	0
12226	F	11.13	1	0	0		1	
10875	M	12.5	1	0	1	1	1	1
1X3929	F	24.24	1		1	0	1	0
1X3947	F	24.01	1	1	1	0	1	0
9089	F	16.34	1		0			
14274	F	7.55						
1X2068	F	26.09						
7455	M	17.94				0	1	0
1X3347	M	25.53						

13715	F	7.58						
1X4277	M	23.25	1	1				
10016	F	14.62	1	1	1	0	1	1
14365	M	7.89						
1X4246	F	22.93	1		1	1	0	0
1X3641	F	25.09	1	0	1	0	1	0
8369	M	17.02	0		1	1	1	1
1X3592	F	25.42	1	0	1	1	0	1
14744	M	6.7				1		1
9388	F	13.76	1		1	1	0	1
8478	F	17.03				1		1
1X3796	M	24.55	1					
8700	F	14.32	1	0	1	1		
1X4056	F	23.74	0	0	0		1	
1X3846	F	24.76	1	0	1			
1X4303	F	22.62	1	0	1	1	0	1
9094	F	14.37	1		1			
7823	F	16.38	1	0	1	1	1	1
1X4112	F	22.34	0	0		1	0	1
10511	F	13.32	1	0	1	0	1	
1X4241	F	20.95	1	0	1			
1X3731	F	24.67	1	0	1	1	1	
1X3895	F	24.67	1	1	0	1	1	1
1X4645	M	20.72	1	1	1	1	1	1
6819	M	18.93	1	1	1	1	1	1
14710	F	11.24	0	1	0	0	1	1
1X3942	F	24.16						
8919	F	14.67	1	1	1			
7096	F	17.37				1	1	1
10046	F	14.4	0	1	0	1		0
7561	F	18.44	1	1	1	1	1	1
15110	M	7.04						
10544	M	13.38						
8596	F	14.41	1	0			1	0
1X4746	F	18.35	0	0	1	0	1	1
1X3861	F	24.03			0	0		1
1X4859	M	19.81	1	1	0			1
6301	M	17.59	1		1			
1X4808	M	20.55				1		
1X3817	F	24.65	1	0	1			
1X2001	F	27.4						
9774	F	13.74				1	0	0
8313	F	16.68	0	1	0	1	1	0

11617	F	11.95		1	1			
1X1927	F	25.78						
13859	F	8.44	1		1	1	0	1
1X4257	F	22.98	0	1	1	1	1	0
1X2825	F	26.37	1	1	1	1	1	1
1X2716	F	26.21	1	1	1	1	1	1
6949	F	18.85	1	1	0	1		0
6933	F	17.63	1		0	1		
1X4276	F	20.8			1			
1X2124	F	27.26						
1X4013	M	22.02		0	1	1	0	0
7944	M	16.15				1		1
9316	F	16.46	1	1	1	1		1
1X4687	F	21.38	1	1	1	1	1	1
11992	F	11.83					0	
14696	F	7.73	0	1	1	1	0	1
1X2684	F	29.82	0	1	1	1	0	0
1X2117	F	25.54	1	0		1	1	0
1X4169	F	23.1	1	0	0	1	1	1
1X4648	M	21.62				1	0	1
9892	M	15.28				1		
1X3810	F	23.52	1	0	0	1	1	1
1X3104	F	23.76	1	1	1	1	0	1
6521	F	20.29				1	0	1
6725	M	17.17	0	0	1	1	0	0
1X1441	F	27.21	1	1	1	1	0	1
1X3914	F	22.16	1	0	1			
1X4239	F	21.06	1	1	1		1	
8001	M	15.99	1		1	1		0
16118	F	6.04	0		1	1		1
7634	F	18.76	1		1	1	1	1
8820	F	15.04			0	1	0	0
16033	F	6.31						
9623	F	13.41	1		1	1	0	1
1X4143	F	24.2	0	0	1	1	1	1
1X3208	F	23.66	1	0	1	1		1
1X4149	F	24.34	1	1	1	1	1	
8318	M	15.31	1		1			
1X4315	M	20.94	1	0	1			
10418	F	11.49	0	0	0		0	
6821	M	17.29	1	1	0	1	1	1
10240	M	12.3	1	0	1		0	1
10009	F	12.6	1		1	1	1	1

9581	F	13.09	1	1	1	1	1	1
1X4867	F	17.85						
8885	M	16.79						
1X4637	M	18.86	0		1	1	0	1
1X3666	F	23.22	0	1	1	1	1	1
1X1557	F	28.91	1	1	1			
9791	F	15.38	1		1	0	1	1
1X1864	F	28.58	1	1	1			
8778	F	16.91	1	0	1	1	1	1
1X4760	M	18.3	1	1	1	1	0	1
7380	M	16.29	1	1	1	1	1	1
1X1577	F	25.96	1	1	1	1	1	0
14754	M	7.9		0				
8292	M	17.84	1	0	1	1	1	1
7158	M	16.67	1	1	1	1	0	1
8644	M	17.4	0		1	0	1	1
10987	F	13.41	1	1	1	1	1	
10911	F	13.55		0	1	1	1	1
1X3836	F	25.44	1	1	1			
9907	F	15.62	1	1	1	1		1
1X3757	M	22.62	1		1	1	0	1
1X4314	F	21	0	1	0	0	1	0
11079	F	13.18	0	0	0	0	1	0
8221	M	15.47	1	0	1	1	1	1
1X2574	F	24.77		1	1			1
1X3749	F	25.45					0	
1X4195	F	21.27	0	1	1	1	1	1
11443	F	17.57	1	1	0			
11445	M	22.67						
6732	F	20.34	0		1	1	1	1
9976	M	15.89	1	1	1	1	0	1
10074	F	15.53	1	1	1	1	1	0
12217	F	11.92	1	1	1	1	1	1
6265	M	20.96				1	1	1
15656	M	7	1	0	1	1	0	1
8780	M	17.45	1	0	1	1	0	1
7430	F	19.44	1	0	1	1	0	0
7190	M	19.67	1	0	1	1	0	1
18744	F	8.55	0	1	1	0	1	1
1X4033	F	24.9			1	1	1	1
1X4721	M	21.73	1	0	1	1	0	0
15988	M	6.73	1	0	1	1	0	1
7438	M	19.24	1	1	1	0	0	1

7438	M	19.24	1	1	1	0	0	1
7438	M	19.24	1	1	1	0	0	0
7438	M	19.24	1	1	1	0	0	0
1X4222	F	24.4	1	0	1	0	1	0
16386	F	6.13			1	1	1	1
14979	M	7.92	1	0	1	1	0	1
15634	M	7.06	1	0	0	1		1
16560	M	6.02	0	1	1	0	0	0
7472	M	19.95				1	1	1
8027	M	18.94	1		0		0	
1X4308	F	23.65	0		1	0	1	1
9805	F	16.57			1	0	1	1
1X4039	F	25.12	1	1	1	1	1	1
1X4082	F	25.23	1	1	1	1	0	1
1X4069	F	25.52	1	0	0	1	1	0
8291	F	18.5	1	0	1	1	0	1
1X4096	M	24.71				1		
1X3926	F	25.87	0	0	1	0	1	1
8299	F	18.52				0	1	1
12480	F	11.96	0		1	1		1
14695	F	8.54	1		1	1		1
8469	M	18.52	1		1	1	0	1
6776	F	25.15		1				1
1X4714	F	18.28	1		1	1		
1X3882	F	25.5	1	1	1	1	1	1
8329	M	18.02			1	1	0	0
1X2100	F	24.96	0	1	1	0	1	1
8034	F	19.16	1	1	0	1	1	1
15155	M	7.77		0	1	1	0	0
6585	M	21.06	1	0	1	1	0	1
6716	M	20.37		1	1	1	1	1
16495	F	6.62	1		1	0	1	1
1X3637	F	26.53	1	0	1		0	1
1X4792	F	21.95		1	0	1	1	1
1X4273	F	23.76		0		0	1	
15976	M	6.97	1		1	1	0	1
1X4121	F	24.68	1	0	1	1	0	1
8008	M	18.33	1		1		1	1
14962	M	7.89						
1X4741	M	11.58				0	0	
1X4006	F	25.03	1	1	1	1	0	1
10740	F	14.39	1		1	1		1
6840	F	20.22	1		1	1	0	1

12466	F	12.12	0	1	1		0	1
13968	M	9.39						
1X4221	M	11.92				1		
14270	F	9.37	1	0	1	1	1	1
13758	F	9.85	1		1	1	1	1
1X4837	F	21.15	1	1	1	1	1	0
8517	M	18.19	0	1	1	1		1
6355	F	21.04	1		1	1	0	1
1X4251	F	24.72	1	0	1	1	0	1
1X4228	F	24.16						
13751	M	10.02	0					
1X3351	F	27.27	1	1	1	1		1
12157	F	12.5	1		1	1	0	
9545	F	17.88				0	1	1
10430	F	16.37	1	1	1	1	1	1
16725	M	7.15	1	1	1	0	1	
15162	F	9.14	1	0	1	1	0	1
9305	F	18.21	1	0	1	1	1	1
8906	M	18.88		0	1	1	1	0
1X4092	F	26.28	0	1	1	1	1	1
1X3786	F	27.48	1	0	1			
10099	F	17.08	1	0		1	0	0
15506	F	8.25	1	1	1	1	0	1
1X3812	F	27.36	1	1	1	0	0	1
9771	F	18.25	1		1	1	0	1
13125	M	12.04				1		1
12411	F	13.25	1	1	1	1	1	1
15538	F	7.66						
15654	M	7.63	0	0	1	1		1
1X4178	F	18.37	1	0	1	1	0	
6802	F	21.81	0	1	1		1	1
1X4866	F	22.06	1	0	1	1	1	1
9356	M	10.46	1	1	1	1		1
1X3687	F	30.16	0	1	1	0	1	1
1X3027	F	28.69	1	0	1	1	1	1
1X2996	F	28.68	0	1	1	1	1	1
9166	F	22.31	1	0	1	1	1	1
7920	F	20.08	1	0	1	1	0	1
6609	M	21.46						
8427	M	19.22	1			1		1
1X3948	F	26.86	1	0	1	0	1	1
7855	F	20.2						
7002	F	21.06	1	1	1	1	1	1

9468	F	17.79	0	0	1	0	0	1
1X4165	F	25.84	1	0	1	1	1	1
16330	M	7.62	1		1	1		1
9969	F	16.61	1	1	1	1	1	1
9092	F	18.12	1	1	1	1	1	1
9338	F	17.98	1	1	1		1	1
9363	F	17.79	1	1	1	1	1	1
7248	F	26.95	0	0	0	0		
1X2361	F	29.42	1	0	1	1	0	1
12175	F	13.32	1	1	1	0	0	1
9515	F	17.85	1	1	1	1	1	1
16576	M	6.65	1	1	1	1	0	1
10153	F	16.57	1	0	1	1	1	
7052	M	21.25	1	0	1	1	0	1
14758	M	9.35						
7210	F	20.52	1	0	1	0	0	1
15828	M	7.61	1	1	1	1	1	1
9326	M	17.62	1		1	1		1
9494	F	17.29	1	1	1	1	1	1
15139	M	8.9						
1X3428	F	27.55	1	1	1	1	1	1
15527	M	8.15	1	0	1	1	0	1
9097	M	18	1	1	1	1	1	1
8615	M	18.81					1	1
17304	F	5.97	1	1	1	1	1	1
15217	M	8.82	1		1	1	0	1
14275	M	10	1		1	1	1	0
26327	F	2.41		1			1	1
10520	F	15.87	1	1	1	1	1	1
9562	M	17.43	1	1	1	1	1	1
8465	M	18.74	1	0	1	1	0	1
2X0236	F	25.84	1	0	1	1	0	1
11015	F	14.69	1	1	1	0	0	1
14995	M	9.09	1	0	1	1	1	1
6222	F	22.94	1	0	1	0		1
6311	F	22.55	1	0	1	1	0	1
1X3765	F	27.59	1	0	1	0	0	1
15584	M	8.65	1	0	1	1	0	1
11001	F	15.37	1	1	1	1	1	1
9656	M	17.85	1	0	0	1	0	1
1X2384	F	29.59	1	1	1	1	0	1
8765	M	19.06	1	0	1	1	0	1
7294	F	21.39	1	0	1	1	1	1

9486	M	18.06	1	1	1	1	0	1
1X4077	F	26.47		0	1	1	0	1
1X3690	F	29.33	0	1	1	1	1	0
1X4642	F	23.87	1	0	1	1	1	1
1X4638	F	23.79	1	1	1	1	1	1
6290	F	22.86	1	1	1	0	0	1
15150	M	9.49	1	1	1	0	1	1
1X4593	F	24.37	1	1	1	1	1	1
1X4213	F	26.08	1	1	1	1	0	1
1X4615	F	24.07	1	0	1	1	0	1
7500	M	20.93	1		1	1		1
7211	F	21.48	0	1	1	0	0	1
6342	F	22.71	1	1	1	1	1	1
18749	F	6.45	1		1	1		1
10509	F	16.52	1	1	1	1	1	1
7963	M	20.16	1	1	1	1	1	1
9265	F	18.47	1	1	1	1	0	1
15444	F	9.09	1	1	1	0	1	1
1X3671	F	29.33	1	1	1	1	1	1
1X3774	F	27.59	1	1	1	1	1	1
1X4052	F	26.77	1	1	1	1	1	1
15283	M	9.31	1	1	1	1	1	1
11769	F	14.04	1	0	1	1	1	1
11439	M	16.33	1	0	1	1	1	1
11581	F	14.87	1	1	1	1	1	1
1X4851	F	21.84	1	1	0	0	1	1
16742	M	7.65	1	1	1	1	1	1
14286	M	10.78	1	1	1	1	0	1
8094	F	20.68	1	0	1	1	1	1
17243	F	7.12	1	1	1	1	1	1
9156	F	19.16	1	1	1	1	0	1
18746	F	7						
7850	M	20.84	1	1	1	1	1	1
9722	F	18.22	1	1	1	1	1	1
1X4736	M	23.88	1	1	1	1	0	1
6668	F	22.36	1	0	1	1	1	1
11499	F	14.63	1	0	1	1	1	1
17214	M	7.31	1	0	1	1	0	1
14204	F	10.97	1	1	1	1	1	1
14508	M	10.58	1	1	1	1	1	1
15539	M	9.44	1		1	1		1
8690	F	19.49	1	0	1	1	1	1
6738	F	22.54	1	1	1	1	1	1

1X4248	F	26.19	1	1	1	1	1	1
8797	F	19.59	1	1	1	1	1	1
9914	F	17.78	1	1	1	1	1	1
1X4779	F	24.01	1	1	1	1		1
6756	F	22.32			1	1	1	1
9278	F	19.23	1	0	1	1	1	1
9576	F	18.88	1	1	1	1	1	1
9625	M	18.8	1	1	1	0	1	1
7267	F	22.06	1	0	1	1	0	1
15293	F	18.89	1	1	1	1	1	1
9340	M	19.14	1	1	1	1	0	1
14044	F	11.28	1	1	1	1	0	1
14983	F	10.13	1	0	1	1	0	1
17331	M	7.18	1			1	0	1
1X4611	F	24.83	1	1	1	1	1	1
8807	M	19.67	1	1	1	1	1	1
14796	M	10.13	1	1	1	1	1	1
9569	F	18.74	1	1	1	1	1	1
12513	F	14.01	1	0	1	1	0	1
6531	F	22.89	1	1	1	1	1	1
2X0331	F	23.83	1	1	1	1	1	1
8623	M	20.07	1	0	1	1	1	1
1X4739	F	23.7	1	1	1	1	1	1
17031	M	7.55	1	0	1	1	1	1
1X3834	M	28.16	1	0	1	1	1	1
6334	M	23.29	1	1	1	1	1	1
9427	M	18.82	1		1	1		1
14665	F	10.5	1	0	1	1	0	0
8895	F	19.7	1	0	1	1	1	1
15639	M	9.07	1	0	1	1		1
6948	F	20.64	1	0	1	1	0	1
1X3849	F	27.99	1	1	1	1	1	1
6714	F	22.48	1	1	1	1	1	1
1X3870	F	27.9	1	1	1	1	1	1
8344	M	20.72	1	1	1	1	1	1
9282	M	19.28	1	1	1	1	1	1
18391	F	6.93	1	0	1	1	1	1
15579	M	9.66	1	1	1	1		1
17355	M	8.06	1	1	1	1	1	1
18341	M	6.79	1	1	1	1	1	1
15140	M	10.33	1	0	1	1	0	1
8827	F	20.23		1	1	1	1	1
8170	M	20.85	1	1	1	1	1	1

7229	M	22.18	1	0	1	1	0	1
15464	F	9.73	1	1	1	1	1	1
11639	F	18.9	1	0	1	1	0	1
10183	F	17.99	1	1	1	1	0	1
14909	F	10.64	1	1	1	1	1	1
10429	F	17.59	1	1	1	1	1	1
8893	F	20.05	1	1	1	1	1	1
6995	F	22.49	1	1	1	1	0	1
7137	F	22.54	1	1	1	1	1	1
1X3649	F	29.48	1	1	1	1	1	1
8980	F	19.93	0	1		0	1	1
8518	M	20.61		0			1	
16368	M	9.05	0	1	1	1	1	1
14167	F	11.59	1	0	1	1	0	1
14499	F	11.65	1	0	1	1	1	1
18971	M	6.7						
15885	F	9.87	0	1	1	0	1	1
14931	F	11.1	0	1	1	1	1	1
11600	F	15.95	0	1	1	1	1	1
9903	M	19.18	1	1	1			
9361	F	19.62	1	1	1	1	1	1
1X4194	F	27.58	1	1	1	1	1	1
8822	F	20.75	1	1	1	1	0	1
6717	F	23.76	1	1	1	1	0	1
6321	M	24.28		0			0	
16115	F	9.7	1	0	1	1	0	1
1X4032	F	28.39	0	1	1			
9714	F	19.6	0	1	1	1	1	1
6315	F	24.48	1	1	1	1	0	1
7735	M	22.21	1	0	1	1	0	1
9174	F	20.35	1	0	1	1	0	1
8574	F	21.18	1	1	1	1	1	1
8274	F	21.59	1	1	1	0	1	1
9495	F	19.99	1	1	1	1	1	1
10128	F	29.15	0	1	1	1	1	1
14883	F	11.39	1	1	1	1	1	1
14859	F	11.5	1	1	1	0	1	1
9586	F	19.89	1	0	1	1	1	1
7606	F	22.4	1	1	1	1	1	1
9128	F	20.44	1	1	1	1	1	1
13280	M	13.33			1			
10208	F	18.42	1	0	1	1	0	1
17230	F	8.5	1	1	1	1	0	1

7784	F	22.13	1	0	1	1	1	1
9285	M	19.89	1	1	1	1	1	1
9417	F	20.07	1	0	1	1	0	1
6800	F	23.76	1	0	1		0	1
7644	F	22.42	1	0	1	1	0	1
8322	F	21.52	1	1	1	1	1	1
7720	F	22.31	1	1	0	1	1	1
8307	F	21.59	1	1	1	1	1	1
15423	F	10.77	1	1	1	1	0	1
6955	M	23.82	0	1	1	1	0	1
8512	F	21.42	1	0	1	1	1	1
2X0252	F	27.45	1	0	1	1	1	1
1X4850	F	24.97	1	0	1	1	1	1
9592	F	20.14	1	1	1	1	1	1
6903	F	23.6	0	0	1	0	0	1
1X4074	F	28.55	1	1	1	1	0	0
1X3830	F	29.49	1	0	1	0	0	1
8134	F	22.01	1	1	1	0	1	1
6753	F	23.96	0	1	1	1	1	1
14676	M	12.06	1	0	1	1	0	1
8860	M	20.49	1	1	1	1	1	1
9129	F	20.43	1	1	1	1	1	1
8826	F	20.84	1	1	1	1	1	1
6838	F	24.09	1	1	0		0	1
8510	F	21.42	1	0	0	1	0	1
7335	F	22.93	1	1	1	1	0	1
7862	F	22.07	1	1	1	1	0	1
8246	F	21.64	1	1	1	1	1	1
1X4272	F	27.41	1	1	1	1	1	1
17966	F	7.98	0	1	1	1		1
15858	F	10.14		1	1	0		1
7368	F	22.89	1	1	1	1	0	1
1X4558	F	26.14				1	1	1
9632	F	19.79	1	0	1	1	1	1
18729	M	7.19	1		1	1	1	1
7663	M	22.31	1	0	1	1	0	1
8698	M	20.1			1	1	0	
9646	F	19.77	0	1	1	1	1	1
8288	M	21.56						
7872	F	22.07	1	1	1			
14955	F	11.2	1	1	0		0	0
8905	F	20.75	1	1	1	1	1	1
1X4009	F	28.29			1			

8937	M	20.75	1	1	1	0	1	0
6528	F	23.95	1	1	0	1	1	1
8667	F	21.05	1	0	0	1	0	0
7844	M	22.19		0			0	
7394	F	22.71	1	1	1	1	0	0
6312	M	24.3	1	0	1		1	
6600	F	23.87	1	1	1	1	1	0
8627	F	1.17	1	1	0	1	1	1
15973	M	9.92	1		1	1		1
7223	M	22.56	1	1	1	1		1
14387	M	11.39						
15938	F	9.98	0	0	1	1	0	1
6734	F	23.7	1	1	1	0	0	0
10157	F	18.64	1	0	1	1	0	1
8092	F	21.67	1	0	1	1		1
12499	F	14.08		1	1	1	1	1
7538	F	21.61	0		1	0	0	1
14894	F	11.14	0	1	1		1	
6280	F	23.77	0	1	1		0	1
9261	M	19.24	0	1	1	1	1	1
12720	F	13.25	1		1	1	0	
16073	M	8.95					1	
6937	F	22.19	1		1	1		1
8786	F	19.6	1	1	1	1	1	1
1X4609	F	24.87	1	1	1	1	0	1
14166	M	11.46	1	1	1	1	0	1
18795	M	6.32	1	1	1	1	0	0
12457	F	14.27	1	1	1	1		0
16102	F	9.47	1	1	0	1	0	1
8212	M	20.77		1	1	0		1
UN009	F			1	1		0	0
14879	F	10.07	1			1		1
8088	F	20.73	1	1	1	0	1	1
16231	F	8.64	1			1		0
17810	F	13.13	1		1	0		1
10044	F	17.95	0		1	1	0	0
11886	F	14.52		0	0	1	0	0
8601	M	19.99	1		0	1	1	1
18747	F	6.08	1					1
7196	F	21.54	1	0	1	1		1
10054	M	18.1	1		0	1		1
9362	F	20.5	1	0	1	1	1	
9514	F	20.35	1	1		1	1	1

8091	M	22.35	1	0	1	1		1
9178	F	20.83	1	1	1		0	0
7017	F	24.44	1	0	1	0	1	1
10039	F	20.12	1	1	1	1		1
10164	F	19.91	1	0	1	1	0	
18531	M	7.82	1	0	0	1	0	
10042	F	19.88	1	1	1	1	1	1
10082	F	20.06	1	1	1	1	0	1
7675	F	22.86	1	1	1	1	1	1
11163	F	17.88		0	1	1	1	1
10535	F	20.07	1	0	1	1	1	0
9040	F	21.04	1	1	1	1	1	1
14923	F	12.32	0	0	0	1	0	1
10130	F	19.76	1	1	1	1	0	0
9694	F	20.33	1		1	1	1	1
8538	F	21.64	0	1	1	1	0	0
6956	F	24.05	1	1	1	1	0	1
13947	M	13.64	1	1	0	1	1	1
11627	F	16.89		0	1	1	1	1
9743	F	20.34	1	1	1	1		1
10259	F	19.56	1		1	1	1	1
10173	M	19.67	1		1	1	0	1
10280	F	19.54	1	1	1	1	0	1
18737	F	12.24		1	0	1		1
9385	F	20.75	1		1		0	1
14478	F	12.34				1	0	1
8183	F	22.39	1	0	1	0	0	0
10297	F	19.47	1	0	0	1	1	1
9124	M	20.98			1		0	1
10161	M	19.79	1			1	0	0
10417	M	19.14						
7764	F	22.74	1	1	1	1	0	1
6793	F	24.57	1	1	1	1	1	1
8926	F	21.25	1		1	1	0	1
9635	F	20.34	0	0	1	0	1	1
9675	F	20.2	0	1	1		1	1
14381	F	12.47	0		1	1	0	1
10393	F	19.26	1	0	1	1		1
15588	M	11.25	1	1	1	1	0	1
7366	F	23.35	1	1	1	1	1	1
10041	M	19.98	0	0	1	1	0	1
10734	F	18.68	0	1	1	0		1
10619	F	19.07	1	0				0

8499	F	21.96	0		1	0	1	1
15674	M	10.75						
9666	F	20.22	1	1		1	1	0
17111	F	9.24	1	1		1	1	1
10127	F	19.97	1		1	1	1	1
10988	F	18.35	1	1	1	1	1	1
10841	F	18.39	1			0		1
11997	F	16.63	0	1	0	0	1	1
10492	F	19.2	1	1	1	0	0	0
14277	M	13.21	1					0
10741	F	18.65	1	1	1			
10160	F	19.88	0	1	1	0		1
9467	F	20.54	0	1	1	0	1	1
15843	F	11.25	1	1	1	1	1	1
11009	F	18.22	1	0	1	1	0	1
10120	F	19.62	1	1	1	1		1
10728	F	18.68	0			0	0	0
10206	F	20.02	0	1	1	1	1	1
10806	F	18.51						
13645	M	14.12		1	1	1	0	1
13625	F	14.23	1	1	1	1		0
11687	F	17.18	1	0	1	1	0	0
9855	F	20.6	0	0	1	0	0	1
10912	F	18.4	1	1	1	0	1	1
10347	F	19.36	0	1	1	1	0	1
10504	F	18.99	1	1	1	1	1	0
14324	F	13.19	0	0	1	0	0	1
11619	F	17.13	1		1	1		1
18742	F	19.14	0	1	1		1	
14039	M	13.55				0		1
9860	M	20.43						
10872	F	17.22	1	1	1	1		1
16852	F	8.99			1			
9205	F	19.97	0	1	1	0		1
7808	F	22.28	0	0	0	1		1
6812	F	23.64						
9014	F	20.59	0			0		1
6740	F	23.72	1	0	1	1		1
7716	F	22.31	1	1	1	1	1	1
7701	F	22.29		1	1	1	0	1
9711	F	19.65	1	1	1	0	0	1
9808	F	19.48	0	0	1			
8116	F	21.87	1	1	1	1	1	1

6971	F	23.58	0	1	1	1		1
8477	M	21.32				1		
8024	M	22.32	1	0	1	1	0	1
12417	F	15.21	0	1	1	1	0	1
7091	M	23.4						
1X4218	F	28.02	1	1	1	0	1	1
1X4243	F	27.8	0	1	1	0	0	0
6622	F	24.13	0	0	0	1	0	1
9841	F	19.59	0	1	1	0	1	1
7398	F	23.03	1	1	1	1	1	1
11672	M	15.61						
13226	F	13.87	0	1	1	0	1	1
13546	M	13.44	1		1	1		
8206	F	22.1	0	0	1	0	1	1
2X0253	F	27.45	1		1	1	0	1
6335	F	24.53	1	1	1	1	1	1
8817	F	21.29	1	1	1	1	1	1
7122	F	23.58	1	0	1	1	0	1
10052	F	19.48	1	0	1	1	1	1
7311	F	23.31	1	1	1	0	0	1
9203	F	20.64	1	1	1	1	1	1

The hemisphere on which the non-netric trait was collected is logged by prefacing the trait name with L (Left) or R (Right). The traits arsp_yn and spcd_yn assess the presence or absence of the arsp and spcd sulci on either hemisphere. The trait cs_forked indicates whether the inferior tip of the central sulcus on that hemisphere was forked or unforked. For presence/absence traits, a 1 indicates presence and a 0 absence of that feature. For cs_forked, a 1 indicates that the cs was forked and a 0 that is was unforked.

Table S3 Genetic correlation matrix for sulcal lengths

Trait	arsp	Cs	iar	ips	lf	lu	ps	sar	spcd	sts
arsp	1.000	0.241	-1.000	0.113	-0.185	-0.287	-0.372	-0.507	0.328	-0.223
cs	0.241	1.000	-0.284	0.240	-0.272	0.432	0.185	-0.188	-0.322	-0.613
iar	-1.000	-0.284	1.000	-0.329	0.264	0.470	0.509	-0.251	1.000	-0.605
ips	0.113	0.240	-0.329	1.000	0.741	0.275	0.399	1.000	0.793	0.577
lf	-0.185	-0.272	0.264	0.741	1.000	0.443	0.255	-0.245	1.000	0.836
lu	-0.287	0.432	0.470	0.275	0.443	1.000	0.555	-0.719	0.083	1.000
ps	-0.372	0.185	0.509	0.399	0.255	0.555	1.000	0.118	0.571	0.267
sar	-0.507	-0.188	-0.251	1.000	-0.245	-0.719	0.118	1.000	-1.000	-0.337
spcd	0.328	-0.322	1.000	0.793	1.000	0.083	0.571	-1.000	1.000	1.000
sts	-0.223	-0.613	-0.605	0.577	0.836	1.000	0.267	-0.337	1.000	1.000

Averaged across both hemispheres, created from the extended baboon pedigree.

Table S4 Phenotypic correlation matrix for sulcal lengths

Trait	arsp	cs	iar	ips	lf	lu	ps	sar	spcd	sts
arsp	1.000	0.144	0.049	0.109	0.115	0.099	-0.032	-0.099	0.146	-0.031
cs	0.144	1.000	0.122	0.278	0.232	0.317	0.206	0.109	0.086	0.138
iar	0.049	0.122	1.000	-0.351	-0.014	0.385	0.468	0.511	0.026	-0.328
ips	0.109	0.278	-0.351	1.000	0.491	0.181	0.009	-0.336	0.354	0.487
lf	0.115	0.232	-0.014	0.491	1.000	0.216	0.076	-0.098	0.282	0.604
lu	0.099	0.317	0.385	0.181	0.216	1.000	0.275	0.223	0.160	0.048
ps	-0.032	0.206	0.468	0.009	0.076	0.275	1.000	0.187	0.108	0.119
sar	-0.099	0.109	0.511	-0.336	-0.098	0.223	0.187	1.000	-0.058	-0.398
spcd	0.146	0.086	0.026	0.354	0.282	0.160	0.108	-0.058	1.000	0.242
sts	-0.031	0.138	-0.328	0.487	0.604	0.048	0.119	-0.398	0.242	1.000

Averaged across both hemispheres and based on baboon endocast metric trait measurements.

Table S5 Anatomical similarity matrix based on brain lobe sulcal location

Trait	arsp	cs	iar	ips	lf	lu	ps	sar	spcd	sts
arsp	1	0.6	0.9	0.3	0.3	0.1	0.6	0.9	0.6	0.3
cs	0.6	1	0.6	0.6	0.6	0.3	0.3	0.3	0.6	0.3
iar	0.9	0.6	1	0.3	0.6	0.1	0.6	0.9	0.5	0.3
ips	0.3	0.6	0.3	1	0.6	0.9	0.3	0.3	0.3	0.6
lf	0.3	0.6	0.6	0.6	1	0.3	0.3	0.3	0.3	0.9
lu	0.1	0.3	0.1	0.9	0.3	1	0.1	0.1	0.1	0.6
ps	0.6	0.3	0.6	0.3	0.3	0.1	1	0.6	0.5	0.3
sar	0.9	0.3	0.9	0.3	0.3	0.1	0.6	1	0.6	0.3
spcd	0.6	0.6	0.5	0.3	0.3	0.1	0.5	0.6	1	0.3
sts	0.3	0.3	0.3	0.6	0.9	0.6	0.3	0.3	0.3	1

Visual partitioning of sulci into brain lobe regions is shown in Figure 1.

Table S6 Connectivity similarity matrix

Trait	arsp	cs	iar	ips	lf	lu	ps	sar	spcd	sts
arsp	1.000	0.308	0.865	0.692	0.615	0.385	0.808	0.731	0.538	0.596
cs	0.308	1.000	0.538	0.750	0.500	0.500	0.308	0.000	0.808	0.500
iar	0.865	0.538	1.000	0.769	0.769	0.615	0.577	0.654	0.404	0.692
ips	0.692	0.750	0.769	1.000	0.500	0.500	0.308	0.538	0.192	0.500
lf	0.615	0.500	0.769	0.500	1.000	0.500	0.308	0.462	0.692	0.750
lu	0.385	0.500	0.615	0.500	0.500	1.000	0.385	0.000	0.000	0.500
ps	0.808	0.308	0.577	0.308	0.308	0.385	1.000	0.769	0.192	0.250
sar	0.731	0.000	0.654	0.538	0.462	0.000	0.769	1.000	0.365	0.442
spcd	0.538	0.808	0.404	0.192	0.692	0.000	0.192	0.365	1.000	0.212
sts	0.596	0.500	0.692	0.750	0.750	0.500	0.250	0.442	0.212	1.000

Created from data in Markov *et al.* (2012).

Table S7 Developmental similarity matrix

Trait	arsp	cs	iar	ips	lf	lu	ps	sar	spcd	sts
arsp	1.000	-0.510	-0.267	0.062	-0.871	0.062	0.785	1.000	0.871	-0.669
cs	-0.510	1.000	0.941	0.749	0.750	0.749	0.026	-0.510	-0.750	0.964
iar	-0.267	0.941	1.000	0.915	0.549	0.915	0.301	-0.267	-0.549	0.837
ips	0.062	0.749	0.915	1.000	0.250	1.000	0.605	0.062	-0.250	0.588
lf	-0.871	0.750	0.549	0.250	1.000	0.250	-0.505	-0.871	-1.000	0.871
lu	0.062	0.749	0.915	1.000	0.250	1.000	0.605	0.062	-0.250	0.588
ps	0.785	0.026	0.301	0.605	-0.505	0.605	1.000	0.785	0.505	-0.179
sar	1.000	-0.510	-0.267	0.062	-0.871	0.062	0.785	1.000	0.871	-0.669
spcd	0.871	-0.750	-0.549	-0.250	-1.000	-0.250	0.505	0.871	1.000	-0.871
sts	-0.669	0.964	0.837	0.588	0.871	0.588	-0.179	-0.669	-0.871	1.000

Based on embryonic day of emergence of each landmark sulci. Created from data presented in Sawada *et al.* (2012).